

A Global Study of the Behaviour of Black Hole X-ray Binary Discs

R. J. H. Dunn^{1*†}, R. P. Fender², E. G. Körding³, T. Belloni⁴ and A. Merloni^{1,5}

¹Excellence Cluster Universe, Technische Universität München, Garching, 85748, Germany

²School of Physics and Astronomy, Southampton, University of Southampton, SO17 1BJ, UK,

³AIM - Unité Mixte de Recherche CEA - CNRS - Université Paris VII - UMR 7158, CEA-Saclay, Service d'Astrophysique, F-91191 Gif-sur-Yvette Cedex, France

⁴INAF-Osservatorio Astronomico di Brera, Via E. Bianchi 46, I-23807 Merate (LC), Italy

⁵Max Planck Institut für Extraterrestrische Physik, Giessenbachstraße, 85471 Garching, Germany

5 November 2018

ABSTRACT

We investigate the behaviour of the accretion discs in the outbursts of the low-mass black-hole X-ray binaries (BHXRBS), an overview of which we have presented previously. Almost all of the systems in which there are sufficient observations in the most disc dominated states show a variation of the disc luminosity with temperature close to $L \propto T^4$. This in turn implies that in these states, the disc radius, R_{in} , and the colour correction factor, f_{col} , are almost constant. Deviations away from the T^4 law are observed at the beginning and end of the most disc dominated states, during the intermediate states. Although these could be explained by an inward motion of the accretion disc, they are more likely to be the result of an increase in the value of f_{col} as the disc fraction decreases. By comparing the expected and observed disc luminosities, we place approximate limits on the allowed distances and masses of the BHXRBS system. In a number of cases, the measured distances and masses of the BHXRBS system indicate that it is possible that the black hole may be spinning.

Key words: accretion, accretion discs - binaries: general - ISM: jets and outflows - X-rays: binaries

1 INTRODUCTION

The outbursts of black hole X-ray binaries (BHXRBS) are dramatic and intriguing events. They have the potential for allowing the study of the physical and emission processes close to the event horizon. The accretion process and associated intermittent jet-production results in emission across the electromagnetic spectrum. In the study presented here, we focus on the X-rays, as these arise from the inner parts of the accretion disc and flow. At the other end of the spectrum, the radio emission is thought to arise from a synchrotron emitting jet. Therefore the radio emission is a good tracer of whether a jet is active or not, and the X-rays are good at determining the state of the accretion flow.

In the now commonly-accepted picture of the changes that occur in the BHXRBS system, the BHXRBS spends most of its time in a quiescent state. There the total luminosity of the BHXRBS is very low, in all bands. As the outburst starts, the X-rays are characterised by a hard emission spectrum with a powerlaw slope of $\Gamma \sim 1.5$ - the “hard state”. As the X-ray luminosity rises, the radio luminosity rises in step (Corbel et al. 2000, 2003). The radio spectrum also indicates the presence of a steady jet emitting syn-

chrotron radiation. As the outburst progresses, the disc spectrum becomes increasingly dominant, eventually softening the entire X-ray spectrum as the BHXRBS enters the “soft-state”. This transition is very fast compared to the speed at which the luminosity rose. Over the course of weeks or even months, the disc luminosity and temperature decay (Gierliński & Done 2004), as the disc dominance decreases (Dunn et al. 2010). Eventually the source returns to the “hard-state” and the luminosity continues to fade. For further details on this picture of the progression of BHXRBS outbursts see Fender et al. (2004); Done & Gierliński (2003); Homan & Belloni (2005); Remillard & McClintock (2006); Done et al. (2007); Belloni (2010).

The accretion onto the compact object is what drives their luminosity in X-rays, which arise from the disc, the corona and even the jet (Russell et al. 2010). Studying emission from the disc allows the accretion process, and also the behaviour of the material within the disc as it approaches close to the compact object to be investigated. The standard theory of accretion discs from Shakura & Sunyaev (1973) shows that the accreting material will form a geometrically thin, but optically thick disc, the inner extent of which depends on the spin of the black hole.

Previous studies on the behaviours of the BHXRBS accretion discs have selected those observations where the disc was dominant, in order to ensure that the disc parameters were well

* E-mail: robert.dunn@ph.tum.de

† Alexander von Humboldt Fellow

determined (Gierliński & Done 2004; Done et al. 2007). This allowed a detailed study of the disc emission from well characterised BHXRBs to be carried out. Using the full archival coverage of the *RXTE*¹ satellite, which has been observing BHXRBs for 13 years, we present a study of *all* observations in which a disc was detected using the analysis of Dunn et al. (2010). This allows us to investigate the properties of the disc in the transition periods, between the fully disc-dominated and powerlaw-dominated states, as well as in the disc dominated states.

In Sections 2 and 3 we recap the data reduction procedure presented in Dunn et al. (2008, 2010) and the final BHXRBs which were selected for this study. The behaviour of the disc's temperature and luminosity are discussed in Section 5. The deviations from the expected behaviour of the disc luminosity and temperature are presented in Section 6, where the inner radius of the disc is investigated, and Section 7, where larger departures are linked to the colour temperature correction. In Section 8 we investigate the limits which can be placed on the distances, masses and spins of the BHXRBs from the observations. The degeneracy of the broken powerlaw model with the disc model, and the evolution of the powerlaw in the hard state are presented in Sections 9 and 10.

2 DATA REDUCTION

In the analysis of the disc properties of the sample of BHXRBs presented in this work we use the analysis of *RXTE* data detailed in Dunn et al. (2010). We recap the main points, but refer to Dunn et al. (2008, 2010) for more details.

We use all the available data publicly available in the *RXTE* archive². This gave a baseline of around 13 years to study the evolution of the disc properties during the numerous outbursts observed within that time. All data were subjected to the same data reduction procedure, in order to minimise differences arising from different data reduction routines.

Both the Proportional Counter Array (*PCA*) and High Energy X-ray Timing Experiment (*HEXTE*) data were required when fitting the spectra, as the *HEXTE* data allows the powerlaw to be constrained at high energy when the *PCA* data are dominated by the disc. We followed the procedure outlined in the *RXTE* Cookbook³ using the tools from *HEASOFT*⁴ version 6.6.2.

To reduce variations between observations further, we only use the data from Proportional Counter Unit (PCU) 2 on the *PCA* as this has been on throughout the *RXTE* mission. Our analysis concentrates on the bright periods when the BHXRBs are in outburst, and so we use the bright model background for all data. Lower count rates are more likely in the inter-outburst periods, and so this choice of a single background is unlikely to bias our results.

In order to proceed with the spectral fitting, we require a *PCA* observation with at least 1000 background subtracted counts, and a *HEXTE* observation with either Cluster A or B (or both) with at least 2000 background subtracted counts. The other *HEXTE* cluster has to have at least a positive number of counts⁵. This count restriction is in place to try to ensure that the spectra which are fitted are of

good quality and fit within a reasonable time with well-constrained parameters.

The spectra were fitted in *XSPEC* (v12.5.0an). In order to study the disc parameters in detail, we needed to analyse the spectra to the lowest energies possible. The relation between the channel numbers of the *PCA* instrument and the energies they correspond to has drifted over the 13 years of the mission. However, all channels below number 7 are not well calibrated for spectral analysis. We therefore choose to ignore *PCA* channels ≤ 6 , which corresponds to around 3 keV, but the exact energy has drifted over time (see the *RXTE* documentation). We also ignore *PCA* data > 25 keV, and *HEXTE* data < 25 keV and > 250 keV.

To be able to characterise the state of the BHXRBs as they go through an outburst we fit three types of base model - unbroken powerlaw (POWER, PL), broken powerlaw (BKNPOWER, BPL) and powerlaw + disc (POWER + DISKBB, DPL). These allow the study of the non-thermal component using the POWER/BKNPOWER parameters, and the disc using the DISKBB parameters. To study the presence and change in the iron line we add an optional 6.4 keV gaussian feature to all these spectra, giving in total six models which were fitted. The low energy sensitivity of *RXTE* is insufficient to allow the N_{H} to be determined from the spectra, and so we fix this value to the accepted value for each BHXRB (see Table 1).

From the six fitted models, we select the best fitting one on χ^2 terms. However if this is not the simplest model, we then determine whether the increase in complexity of the model is significant using an *F*-test with $\mathcal{P} < 0.001$ as the significance level. For the complete routine see Dunn et al. (2010), but a quick outline is described below. When the best fitting model is complex but contains no gaussian component, we test this best fitting model against the simple powerlaw result. If the best fitting model is complex and contains a gaussian component we first test whether the underlying complex continuum model is an improvement over the simple powerlaw, and if it is we test whether a line is required in this complex model. When the complex continuum is not an improvement over the simple powerlaw a number of further steps are performed, as detailed in Dunn et al. (2010).

Once the best fitting model has been selected, we further cut the observation number by removing any observation whose 3 – 10 keV flux is less than 1×10^{-11} erg s⁻¹, where the flux was not well determined or where the powerlaw was not well constrained (even if the disc was). The flux cut was performed to focus on the periods in which the BHXRBs are in outburst, and so streamline the data reduction process. We also removed those fits whose $\chi^2 > 5.0$ as these are spectra which are not well fit by any of the models available within our automated procedure. The distribution of the χ^2 of the best fitting models is shown in Dunn et al. (2010) Fig. 2. The majority of fits are clustered around $\chi^2 \sim 1$, but there is a large tail to higher values. As the spectral fitting in this work has been automated, such large tail is expected.

2.1 Model fitting issues

The relatively high lower energy bound for the *RXTE* response limits our ability to detect discs when they are not dominant. The maximum power emitted by the DISKBB model occurs around $2.4kT_{\text{Disc}}$ which is usually around the lower limit of the *PCA* bandpass (for discs at ~ 1 keV). Therefore we rarely detect the peak of the disc emission, and more usually observe the Wien tail. Using a simple powerlaw to model the non-thermal continuum, even when including *HEXTE* data, does not allow for small breaks or curvature within this component. If a disc component was included in these

¹ Rossi X-ray Timing Explorer

² The cut-off date used was the 4 August 2009, as in Dunn et al. (2010).

³ http://rxte.gsfc.nasa.gov/docs/xte/recipes/cook_book.html

⁴ <http://heasarc.gsfc.nasa.gov/lheasoft/>

⁵ The background subtraction procedure for *HEXTE* can result in negative numbers of foreground counts for low fluxes.

observations, it was found to try and fit these small curvatures in the powerlaw rather than any true underlying disc component, resulting in unphysical disc parameters. We therefore limited the minimum temperature for the disc during the fitting to $k_B T = 0.1$ keV. Furthermore we then penalise the χ^2 of any model which has a $k_B T < 0.4$ keV when selecting the best fitting model. We note that in doing this we are limiting our sensitivity to low temperature discs, in the intermediate and hard states for example, and are probably excluding a few accurate disc fits. We investigate further degeneracies between the disc and broken powerlaw models in Section 9.

More complex models, for example Comptonization, would in principle give more information on the state of the system in these disc dominated states, as it links the non-thermal emission to the disc temperature. However, in order to freely fit all the parameters of the Comptonization models a high signal-to-noise observation is required. Not all of our observations have sufficient counts to be able to do this; in fact very few would allow all parameters to be determined from the observations. Although fixing some parameters would allow these models to fit successfully, this goes against the methodology of this work, by *a priori* constraining parameters differently for different states.

3 SELECTED OBJECTS

After all the data reduction, dead-time and selection the 15 Ms of raw *RXTE* data was trimmed to ~ 10 Ms in 3919 observations, with well fitted spectra and high enough fluxes and counts. The sample of objects was not designed to be complete in any way. We selected objects which were well known BHXRBS in the literature as well as those which were known to have outbursts which had been well monitored by *RXTE*. The set of BHXRBS analysed in this sample, along with their physical parameters (where known) and the final number of observations used in this study are shown in Tables 1 and 2.

There are two notable BHXRBS which were purposely not included in this study (e.g. Cyg X1 and GRS 1915-105). These two sources were not included for a number of reasons. One was a purely practical one resulting from the sheer amount of data available for these sources. The reduction of all the observations in the scheme outlined above would have dominated any of the global studies presented both here and in Dunn et al. (2010), and selecting certain parts would have gone against the philosophy of the study, by not including all of the available data. Secondly, the behaviour of these sources is not easily explained by the outburst model presented in Fender et al. (2004). In the following sections, we use this outburst scheme and the states it describes to explain the behaviour of the disc and powerlaw components. As the behaviour of these two well studied BHXRBS do not easily fall fit into this scheme, we actively decided to not include them in the study at this time.

Many of the masses and distances are unknown or not very well constrained. Where they are unknown we have assumed values of $10M_\odot$ and 5 kpc respectively. These uncertainties effect the calculation of the Eddington Luminosities (L_{Edd}) for these BHXRBS which are used extensively throughout this analysis to scale the BHXRBS to one another. Until the distances and masses are well determined, there will always be some uncertainty when comparing between sources.

The investigation presented in this work concentrates on the variation of the disc characteristics during the outburst as the changes in the disc parameters are the most prominent changes in

Table 2. OBSERVATION NUMBERS, TIMES AND DISC DETECTIONS

Object	Selected Obs	Exposure Ms	Disc Detections
4U 1543-47	61	0.147	36
4U 1630-47	704	1.371	491
4U 1957+115	59	0.260	25
GRO J1655-40	484	1.829	368
GRS 1737-31	5	0.045	2
GRS 1739-278	6	0.017	6
GRS 1758-258	9	0.007	9
GS 1354-644	8	0.049	1
GS 2023+338	0	0.000	0
GX 339-4	709	1.682	284
H 1743-322	346	0.998	224
XTE J1118+480	81	0.170	1
XTE J1550-564	365	0.833	168
XTE J1650-500	108	0.191	37
XTE J1720-318	63	0.125	33
XTE J1748-288	21	0.074	12
XTE J1755-324	2	0.006	1
XTE J1817-330	123	0.329	100
XTE J1859+226	121	0.292	101
XTE J2012+381	15	0.036	15
LMC X-1	69	0.349	64
LMC X-3	471	1.048	173
SAX 1711.6-3808	13	0.029	5
SAX 1819.3-2525	48	0.114	2
SLX 1746-331	28	0.091	14
Totals	3919	10.09	2172

the spectrum during a BHXRBS outburst. Our results are therefore dominated by those objects which have had outbursts well monitored by *RXTE*. Roughly this “removes” all the BHXRBS from our study which have only had a few *RXTE* observations. Some objects which have had a comparatively large number of observations are not observed to undergo the canonical outburst structure outlined in Section 1. These sources are less able to show what changes disc undergoes during a complete outburst, but are still useful for the hard/powerlaw dominated states.

4 DISC PARAMETERS

The discs around black holes are thought to be optically thick and geometrically thin (Shakura & Sunyaev 1973). The spectrum expected from this kind of disc around a non-rotating black hole is easily calculated. It is the sum of a set of blackbody spectra, one for each radius, R , with a characteristic temperature $T_{\text{eff}}(R)$. The total spectrum resulting from this sum is then a multicolour disc blackbody, with a peak temperature $T_{\text{eff,max}}$ coming from close to the innermost stable orbit. However, this spectrum is effected by the opacity of the disc, which results in a colour temperature correction factor, f_{col} (Shimura & Takahara 1995; Merloni et al. 2000; Davis et al. 2006). This factor was shown by Shimura & Takahara (1995) to be ~ 1.8 for almost all black hole masses and emission luminosities and is discussed further in Section 7. Of course, the description of the disc may not be quite as simple as envisaged by Shakura & Sunyaev (1973) and radiatively inefficient flows (e.g. Advection Dominated Accretion Flows, Ichimaru 1977; Narayan & Yi 1994) or slim discs (e.g. Abramowicz et al. 1988)

Table 1. X-RAY BINARY PARAMETERS

Object	M_{BH} (M_{\odot})	D (kpc)	N_{H} ($\times 10^{22} \text{ cm}^{-2}$)	P_{orb} (h)	M_{*} (M_{\odot})	Inclination ($^{\circ}$)
4U 1543-47	9.4 ± 2.0 (1,2)	7.5 ± 0.5 (3,4)	0.43 (2,4)	26.8 (4)	2.45 (1)	21 (2)
4U 1630-47	[10]	10.0 ± 5.0 (5)	> 6 (6)	–	–	–
4U 1957+115	[10]	[5]	0.15 (7)	9.3 (8)	1.0 (9)	–
GRO J1655-40	7.0 ± 0.2 (10,11)	3.2 ± 0.2 (4,12)	0.8 (13)	62.9 (4)	2.35 (10)	70 (48)
GRS 1737-31	[10]	[5]	6.0 (14)	–	–	–
GRS 1739-278	[10]	8.5 ± 2.5 (15)	2 (15)	–	–	–
GRS 1758-258	[10]	[5]	1.50 (16)	18.5 (17)	–	–
GS 1354-644	$> 7.8 = 10.0 \pm 2.0$ (1)	$> 27 = 33 \pm 6$ (18)	3.72 (18,19)	61.1 (18)	1.02 (1)	–
GS 2023+338	10 ± 2 (1)	4.0 ± 2.0 (4)	0.7 (4)	155.3 (4)	0.65 (1)	–
GX 339-4	5.8 ± 0.5 (20)	8.0 ± 4.0 (21)	0.4 (22)	42.1 (4)	0.52 (20)	40
H 1743-322	[10]	[5]	2.4 (23)	–	–	–
XTE J1118+480	6.8 ± 0.4 (1,24)	1.7 ± 0.05 (25,26)	0.01 (25)	4.08 (4)	0.28 (1)	68 (26)
XTE J1550-564	10.6 ± 1.0 (3)	5.3 ± 2.3 (4)	0.65 (27)	37.0 (4)	1.30 (3)	72 (3)
XTE J1650-500	$< 7.3 = 6 \pm 3$ (28)	2.6 ± 0.7 (29)	0.7 (30)	7.7 (28)	–	30 (49)
XTE J1720-318	[10] (31)	$> 8 = 8 \pm 6$ (31)	1.24 (31)	–	–	–
XTE J1748-288	[10]	$> 8 = 10 \pm 2$ (32)	7.5 (33)	–	–	–
XTE J1755-324	[10]	[5]	0.37 (34)	–	–	–
XTE J1817-330	$< 6 = 4 \pm 2$ (35)	$> 1 = [10]$ (35)	0.15 (35)	–	–	–
XTE J1859+226	10 ± 5 (36)	6.3 ± 1.7 (4)	0.34 (36)	9.17 (4)	0.9 (36)	–
XTE J2012+381	[10]	[5]	1.3 (37)	–	–	–
LMC X-1	10 ± 5 (38)	52 ± 1.0 (39)	0.5 (13)	93.8 (40)	–	45 (38)
LMC X-3	10 ± 2 (41)	52 ± 1.0 (39)	0.06 (42)	40.8 (43)	6 (41)	60 (41)
SAX 1711.6-3808	[10]	[5]	2.8 (44)	–	–	–
SAX 1819.3-2525	10 ± 2 (46)	10 ± 3 (46)	0.1 (47)	67.6 (46)	–	65 (46)
SLX 1746-331	[10]	[5]	0.4 (45)	–	–	–

Many of the objects do not have well determined distances or masses. In this case we have taken the distances to be 5 kpc and the masses $10 M_{\odot}$. A recent critical look at the distance estimates for GRO J1655-40 by Foellmi (2009) indicates a revised estimate of the distance of < 2.0 kpc. References:

(1) Ritter & Kolb (2003), (2) Park et al. (2004), (3) Orosz et al. (2002), (4) Jonker & Nelemans (2004), (5) Augusteijn et al. (2001), (6) Tomsick et al. (2005), (7) Nowak et al. (2008), (8) Thorstensen (1987), (9) Shahbaz et al. (1996), (10) Hynes et al. (1998), (11) Shahbaz et al. (1999), (12) Hjellming & Rupen (1995), (13) Gierliński et al. (2001), (14) Cui et al. (1997), (15) Greiner et al. (1996), (16) Pottschmidt et al. (2006), (17) Smith et al. (2002), (18) Casares et al. (2004), (19) Kitamoto et al. (1990), (20) Hynes et al. (2003), (21) Zdziarski et al. (2004), (22) Miller et al. (2004), (23) Capitanio et al. (2005), (24) Wagner et al. (2001), (25) Chaty et al. (2003), (26) Gelino et al. (2006), (27) Gierliński & Done (2003), (28) Orosz et al. (2004), (29) Homan et al. (2006), (30) Miniutti et al. (2004), (31) Cadolle Bel et al. (2004), (32) Hjellming et al. (1998), (33) Kotani et al. (2000), (34) Revnivtsev et al. (1998), (35) Sala et al. (2007), (36) Hynes et al. (2002), (37) Campana et al. (2002), (38) Hutchings et al. (1987), (39) di Benedetto (1997), (40) Orosz et al. (2008), (41) Cowley et al. (1983), (42) Haardt et al. (2001), (43) Hutchings et al. (2003), (44) in't Zand et al. (2002), (45) Wilson et al. (2003), (46) Orosz et al. (2001), (47) in't Zand et al. (2000), (48) van der Hoof et al. (1998), (49) Sanchez-Fernandez et al. (2002)

may exist. However, we concentrate on the disc model proposed by Shakura & Sunyaev (1973) in this study.

We use the physical description in Gierliński & Done (2004); Gierliński et al. (1999) to calculate the relation between the disc luminosity and the temperature as for a Schwarzschild black hole,

$$\frac{L_{\text{Disc}}}{L_{\text{Edd}}} \approx 0.583 \left(\frac{1.8}{f_{\text{col}}} \right)^4 \left(\frac{M}{10 M_{\odot}} \right) \left(\frac{kT_{\text{max}}}{1 \text{ keV}} \right)^4, \quad (1)$$

which assumes a constant inner disc radius, R_{in} . We investigate the effects of the black hole spin in Section 8. We include the adjustments to the observed disc temperature, T_{obs} , for relativistic effects close to the black hole (Gierliński & Done 2004). We add a 4 per cent temperature shift to account for the stress-free boundary layer, and also the adjustment from Zhang et al. (1997) which accounts for the strong gravitational potential.

$$T_{\text{max}} = T_{\text{obs}} / f_{\text{GR}}(\theta, a^*) \xi,$$

where $\xi = 1.04$ is for the stress-free boundary layer, θ is the inclination angle and a^* the dimensionless spin parameter. Out of the ~ 3900 observations ~ 2200 have disc detections (see Table 2). Although the number of observations in which a disc is well determined depends on the state of the BHXRB at the time it was

observed, we show the number of disc detections so that it is clear that a few BHXRBs have many more detections than most of the others. Therefore our conclusions are depend more on the results from these BHXRBs.

In the data reduction routine and best fitting model selection procedure we have been conservative in determining which observations have discs (see Section 2.1). Initially we investigate the degree to which the BHXRB discs follow the expected $L - T$ relation (Equation 1), using an $f_{\text{col}} = 1.8$ and assuming that the inner radius of the disc is constant. In later Sections we relax these assumptions.

In the following, we define the Powerlaw Fraction (PLF) and the Disc Fraction (DF) as

$$\text{PLF} = \frac{L_{1-100 \text{ keV, PL}}}{L_{0.001-100 \text{ keV, Disc}} + L_{1-100 \text{ keV, PL}}}$$

$$\text{DF} = \frac{L_{0.001-100 \text{ keV, Disc}}}{L_{0.001-100 \text{ keV, Disc}} + L_{1-100 \text{ keV, PL}}},$$

following Dunn et al. (2010) as well as Dunn et al. (2008); Körding et al. (2006). These two quantities, used when creating Disc Fraction Luminosity Diagrams, allow the natural separation of the outburst into two states - powerlaw and disc dominated. These

correspond roughly to the hard and soft states more commonly used in BHXRB studies. For an in depth study of the relation between these state conventions see Dunn et al. (2010).

5 DISC TEMPERATURE AND LUMINOSITY

We show the variation of the disc temperature with unabsorbed disc luminosity for each BHXRB individually in Appendix Fig. A.1. The errorbars are only from the uncertainties arising in the spectral fitting. We do not include the uncertainties in physical parameters of the BHXRB system (e.g. mass and distance), as in many cases the physical parameters are unknown, and would further complicate the diagram. We also show the theoretically expected $L - T$ relation for $f_{\text{col}} = 1.8$ for each BHXRB on each diagram in Appendix Fig. A.1 as the dashed black line, using the masses as shown in Table 1 (again without including the uncertainties). Also shown in Appendix Fig. A.1 is a schematic showing the motion of the BHXRB through the $L - T$ plane as an outburst progresses. For clarity, for the remainder of this section the theoretical $L - T$ relation is that from Eq. 1 under the assumption of a constant inner disc radius and colour correction factor.

In Appendix Fig. A.1 it is clear that most of the BHXRB’s discs do closely follow the theoretically expected $L - T$ relation. We fit the most disc dominated points ($DF > 0.8$) of each BHXRB with a powerlaw in the $\log_{10} T - \log_{10} L_{\text{Disc}}$ plane, where for a constant size black body a slope of four is expected. We show the resulting slopes in Table 3 and a histogram of their distribution in Fig. 1. The best-fit Gaussian distribution to the histogram peaks at a slope of 4.48. We select the most disc dominated observations in order to focus on those where the disc parameters (temperature and disc normalisation in XSPEC) were very well determined and also to exclude points close to the intermediate state, where the relation may not apply (similar to the selection performed in Gierliński & Done 2004). The behaviour of the disc temperature at smaller disc fractions, corresponding to states closer to the intermediate states, and are discussed in Section 7.

Of the ten BHXRBs studied by Gierliński & Done (2004), nine are included in our study. For four of the BHXRBs, their distribution of observations match between their study and those in Appendix Fig. A.1 (GRS 1739-278, XTE J2012+381, LMC X-1 and LMC X-3). There are many more observations of GX 339-4 presented in our study, and so it is difficult to determine any differences between the two studies. Of the remaining four BHXRBs (GRO J1655-40, XTE J1550-564, XTE J1650-500 and XTE J1859+226), the trends observed in Gierliński & Done (2004) show very clear and linear $\sim T^4$ relations. However, in Appendix Fig. A.1 we find that, although the most disc dominated observations do on the whole follow the expected $L - T$ relation, there are a large number of points at low disc fractions which fall “below” the expected $L - T$ relation (see also Section 7). In this study, we include and show all observations in which a disc+powerlaw model was the best fit, whereas those in Gierliński & Done (2004) select “disc dominated spectra” where up to 15 per cent of the total bolometric emission can be present in a Comptonized tail. In Appendix Fig. A.1 we only fit those observations for which $DF > 0.8$ and therefore the apparent observed differences are large because of the plotted low disc fraction points.

In a number of the BHXRBs, the statistically best fitting line is not similar to the expected $L - T$ relation. This mismatch in between the slopes of the expected $L - T$ relation and that of the best fit to the most disc dominated states could arise from the lim-

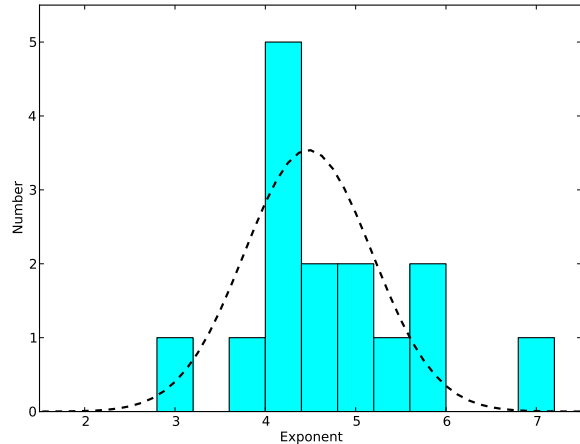


Figure 1. The distribution of the best fitting slopes in the most disc dominated states. The indicated Gaussian is a least-squares fit to the histogram, and peaks at 4.48 with a width of 0.33. GRS 1739-278, XTE J1650-500 and LMC X-1 are beyond the edges of the plot (see Table 3).

itations on the range of disc temperatures probed and the spectral response of *RXTE*. If only a few observations have a detected disc, then the variation in the disc temperature and luminosity may be small, which could mask a T^4 trend if the scatter is naturally high, for example GRS 1739-278 and LMC X-1.

In a large number of cases, although the shape of the relation is close to that of the $L - T$ relation, the normalisations are not always correct (see Equation 1). Given the uncertainties in the masses and distances an offset between the observed and expected behaviours is not unexpected. We also note that the expected $L - T$ relation assumes that the black hole is not spinning. We discuss the effects of these unknown system parameters further in Section 8.

Therefore it is clear that under the assumption of a constant f_{col} and a constant inner disc radius, R_{in} , the majority of the BHXRBs show a variation of the disc luminosity, $L_{\text{Disc}} \propto T^4$ in the most disc dominated states over an order of magnitude in luminosity and a factor of two in disc temperature. This has been found by earlier studies (e.g. Gierliński & Done 2004; Davis et al. 2006; Dunn et al. 2008), though in some cases the analysis as restricted to the most disc dominated (soft) states. Specifically, the ratio of $R_{\text{in}} : f_{\text{col}}$ is constant in these states. However, it would be very strange if the dynamics of the accretion disc and the radiation transfer processes conspired to keep this ratio constant, and so it is likely that each quantity is itself, constant, in the disc dominated state. However, what of the behaviour in the less disc dominated states? As noted above, many of the observations at low disc fractions fall “below” the expected “L-T” relation. We investigated whether this could result from slightly different $L - T$ relations from different outbursts of the same BHXRB, however no clear or variation was found. A number of the low disc fraction observations are seen as almost perpendicular deviations from the expected $L - T$ relation. The trend for these “spurs” is for the disc luminosity to decrease as the disc temperature increases and are observed both at the beginning and the end of the outbursts (see e.g. 4U 1543-47 and GRO J1655-40). We discuss these deviations further in Section 7.

There are a few cases where the best fit line to the most disc dominated observations is radically different to the expected $L - T$ relation even though there are a large number of observations, e.g.

XTE J1650-500, LMC X-1. It is almost as if whatever is causing the “spurs” dominates the variation of the disc temperature and luminosity in these objects. In these two BHXRBS there are two effects which conspire to give best-fit relations different to the expected $L \propto T^4$. Firstly, in both of these sources the majority (if not all) of observations have the same luminosity. In XTE J1650-500 those observations occur just after the disc fraction reaches 0.8, rather than in the most disc dominated state of the outburst ($DF > 0.9$). If we select those observations with $DF > 0.9$ as opposed to $DF > 0.8$ then the slope of the best fitting line is 9.52. Whereas in LMC X-1 the only a few observations have a sufficiently high disc fraction to be fitted, with almost no variability in the total luminosity⁶. Secondly, as seen in a number of the other BHXRBS, observations at intermediate states, or those which do not have overly strong disc fractions show “spurs” running approximately perpendicular to the $L - T$ relation. Both of these effects are combined with the scatter observed in the the relations exhibited by other BHXRBS.

Therefore, if there are few points in the most disc dominated states (XTE J1650-500) or there is a small variation in the luminosity (LMC X-1), it is possible that the best fit relation will not be close to the theoretically expected one. However, in XTE J1650-500, the best fit relation to the observations with $DF > 0.9$ is much closer to the expected $L - T$ relation. In a study of the discs in BHXRBS Gierliński & Done (2004) also find that LMC X-1 does not appear to follow the relation. However the range in disc temperatures and luminosities in their study, like the observations presented here, is comparatively small. XTE J1650-500 is also included in their study, and although they find departures from the $L_{\text{Disc}} \propto T^4$ law, these observations have large error bars and so are consistent still with it.

The theoretical $L - T$ relation depends on the mass of the BHXRBS - which can reasonably be assumed to be constant during the outburst - the f_{col} , the colour temperature correction factor, the spin and also the inner radius of the disc, R_{in} . The behaviour of the disc temperature and luminosity seen in Appendix Fig A.1 for the majority of the observations of the BHXRBS, indicates that over a large range in disc temperature and luminosity, both the f_{col} and R_{in} are relatively constant, at least in the most disc dominated states. There is some scatter around the best fitting relation which on the whole appears random with no clear secondary trend (see Fig. 1). However, in the “spurs” at the beginning and ends of the outbursts, the deviation from the $L - T$ relation is large, and we now investigate whether coherent variations either R_{in} or f_{col} could cause them.

6 DISC RADIUS

Only when the inner radius of the disc, R_{in} , is constant will the disc luminosity and temperature follow the expected $L \propto T^4$ relation assuming that f_{col} is also constant. As we have shown in Section 5 that for the majority of the observations the expected $L - T$ relation

⁶ We note that the not all of the best fitting models appear appropriate for LMC X-1 in Dunn et al. (2010), as all the observations have similar X-ray colours, yet some have no disc component as seen in the Disc Fraction Luminosity Diagram (see Körding et al. (2006); Dunn et al. (2008) and Dunn et al. (2010) for more details). This is likely to be the result of the similarity between a broken powerlaw model and a disc + powerlaw model when the disc does not dominate the spectrum. This is exacerbated in LMC X-1 as the hard X-rays are also faint as a result of the large distance to the BHXRBS, which make fitting the powerlaw difficult.

Table 3. DISC TEMPERATURE FITS

Object	Exponent	Points	Note
4U 1543-47	5.76 ± 0.76	26	
4U 1630-47	5.67 ± 0.23	245	
4U 1957+115	4.10 ± 0.24	16	
GRO J1655-40	4.16 ± 0.14	209	
GRS 1737-31	–		
GRS 1739-278	-0.59 ± 0.02	5	1
GRS 1758-258	4.80 ± 0.42	2	
GS 1354-644	–		
GS 2023+338	–		
GX 339-4	7.08 ± 0.37	197	
H 1743-322	3.70 ± 0.14	99	
XTE J1118+480	–		
XTE J1550-564	4.26 ± 0.09	109	
XTE J1650-500	24.64 ± 7.79	28	2
XTE J1720-318	5.21 ± 0.19	29	
XTE J1748-288	3.19 ± 0.16	5	
XTE J1755-324	–		
XTE J1817-330	4.68 ± 0.23	88	
XTE J1859+226	4.11 ± 0.34	52	
XTE J2012+381	4.28 ± 0.55	15	
LMC X-1	-1.88 ± 0.88	14	3
LMC X-3	4.64 ± 0.11	109	
SAX 1711.6-3808	–		
SAX 1819.3-2525	–		
SLX 1746-331	4.88 ± 0.40	12	

The number of points are those used in the fitting, so with a Disc Fraction > 0.8 . Notes: 1 – GRS 1739-278 has very few points for the fitting. 2 – XTE J1650-500 has a strange distribution of observations along the outburst, causing the erroneous fit. 3 – LMC X-1: small range in disc temperatures and luminosities and the slope is not well defined.

is a good description of the behaviour, then we expect that the disc radius remains constant for the most disc dominated observations.

To calculate the disc radius, we use the normalisation of the DISKBB model, \mathcal{N} , from XSPEC as this explicitly includes the inner radius of the disc, R_{in} .

$$\mathcal{N} = \left[\frac{R_{\text{in}}}{D_{10 \text{ kpc}}} \right]^2 \cos \theta, \quad (2)$$

where $D_{10 \text{ kpc}}$ is the distance in units of 10 kpc and θ is the inclination of the system. Where the inclination of the system is not known (Table 1) we use $\theta = 60^\circ$. It is possible that the discs in some of these BHXRBS are misaligned with respect to the binary’s inclination (Maccarone 2002; Fragos et al. 2010). In Appendix Fig A.1 we show the inner radius against the disc temperature for each BHXRBS. We do not include the effect of the uncertainties in the distance and inclination in the error bars shown. We also show in Appendix Fig A.1 a schematic diagram demonstrating the motion of the BHXRBS through the $R_{\text{in}} - T$ plane as the outburst progresses. As, on the whole, the disc temperature decays during the most disc dominated stages of the outburst, the track of the BHXRBS through the $R_{\text{in}} - T$ plane should be clear.

As was expected from the behaviour of the disc luminosity and temperature, and from the study of GX 339-4 by Dunn et al. (2008), the majority of points are at a relatively constant inner disc radius. We have chosen to plot the disc radius in kilometres on the primary x -axis rather than R as fractions of the gravitational radius, R_g , as in many of the BHXRBS the masses are not accurately known. The secondary x -axis shows the radii as a fraction of R_g .

Table 4. DISC INNER RADIUS FITS

Object	R_{in} (km)	$R_{\text{in}}/R_{\text{g}}$
4U 1543-47	$53.6^{+10.4}_{-8.7}$	$3.86^{+0.75}_{-0.62}$
4U 1630-47	$20.9^{+3.6}_{-3.1}$	$1.42^{+0.24}_{-0.21}$
4U 1957+115	$2.43^{+0.07}_{-0.07}$	$0.16^{+0.005}_{-0.005}$
GRO J1655-40	$21.8^{+2.1}_{-1.9}$	$2.11^{+0.21}_{-0.19}$
GRS 1739-278	$29.3^{+0.6}_{-0.6}$	$1.98^{+0.04}_{-0.04}$
GRS 1758-258	$4.90^{+0.01}_{-0.01}$	$0.33^{+0.0009}_{-0.0009}$
GX 339-4	$42.0^{+8.6}_{-7.1}$	$4.90^{+1.00}_{-0.83}$
H 1743-322	$22.4^{+2.2}_{-2.0}$	$1.52^{+0.15}_{-0.14}$
XTE J1550-564	$49.4^{+5.4}_{-4.8}$	$3.15^{+0.34}_{-0.31}$
XTE J1650-500	$18.9^{+4.3}_{-3.5}$	$2.14^{+0.49}_{-0.40}$
XTE J1720-318	$69.5^{+16.7}_{-13.4}$	$4.70^{+1.13}_{-0.91}$
XTE J1748-288	$28.2^{+1.4}_{-1.3}$	$1.91^{+0.09}_{-0.09}$
XTE J1817-330	$66.2^{+12.9}_{-10.8}$	$11.12^{+2.18}_{-1.82}$
XTE J1859+226	$35.5^{+6.5}_{-5.5}$	$2.40^{+0.44}_{-0.37}$
XTE J2012+381	$27.2^{+1.4}_{-1.4}$	$1.84^{+0.10}_{-0.09}$
LMC X-1	$38.2^{+5.6}_{-4.9}$	$2.59^{+0.38}_{-0.33}$
LMC X-3	$36.1^{+2.1}_{-2.0}$	$2.44^{+0.14}_{-0.14}$
SLX 1746-331	$6.7^{+0.7}_{-0.7}$	$0.45^{+0.05}_{-0.04}$

The inner radius estimates do not include the uncertainties on the values or estimates on the distance or mass of the BHXR (see Equation 2). As a reminder, the inner radius of the disc is $6R_{\text{g}}$ for a non-rotating black hole, and $1R_{\text{g}}$ for a maximally rotating one.

for comparison. We show in Table 2 the best fit inner radii for the observations with a Disc Fraction > 0.8 .

In some BHXR (4U 1957+115, GRS 1758-258 and SLX 1746-331) the disc radii are very small, less than 10 km or below $1R_{\text{g}}$. The innermost stable circular orbit (ISCO) for a black hole is $6R_{\text{g}}$ for a non-rotating black hole, where $R_{\text{g}} = GM/c^2 =$ is the Schwarzschild radius. For a maximally rotating black hole, the ISCO can go down to R_{g} . In these three BHXR the distances, masses and inclinations are not known, and so these effect the estimates on the inner disc radius. From the normalisation, \mathcal{N} , the distance is directly proportional to the R_{in} , the mass inversely proportional (when measured in units of R_{g}) and the inclination has a $(\cos \theta)^{-1/2}$ dependence. The most change would arise if the inclination would increase, though increasing the distance or decreasing the mass would also increase the inner disc radius. However, not knowing the true values of the inner disc radius, it is difficult to determine which of these parameters should change and by how much. Therefore, although the estimates on the inner disc radius are smaller than physically sensible, it is likely to be the result of our incomplete knowledge of the system parameters.

The ‘‘spurs’’ which were mentioned in Section 5 are also seen in the $R_{\text{in}} - T$ plots. If taken at face value, then they indicate that at the end of the outburst the inner disc radius decreases as the disc temperature rises, and vice versa at the beginning of the outburst. This behaviour does not appear to be physically meaningful, as the minimum radius measured for some of the observations fall well within the smallest stable orbit for a $10M_{\odot}$ black hole. We discuss these spurs and their possible causes further in the following section.

7 THE SPURS - AN F_{COL} CONNECTION?

As has been alluded to in the above sections, apart from the theoretically expected $L - T$ relation at constant disc radius R_{in} , the

other main trend is perpendicular to the $L_{\text{Disc}} \propto T^4$ relation, leading to an apparent decrease in the disc radius at the beginnings and ends of the outburst. These spurs are seen in most of the BHXR, and were also seen in GX 339-4 in Dunn et al. (2008), XTE J1650-500 in Gierliński & Done (2004) and GRO J1655-40 in Done et al. (2007).

The plots of $R_{\text{in}} - T$ in Appendix Fig. A.1 show that the disc radius decreases to very small values at the beginnings and ends of the outbursts. It is the extent of the decreases, down to values well below $1R_{\text{g}}$, that lead us to investigate whether changes in f_{col} could be responsible. Although changing the system parameters can shift the location of the observations in the $R_{\text{in}} - T$ plane, they are unlikely to move the observations with the smallest calculated R_{in} sufficiently far. We note that there are also points which occur at quite a distance from the main $L - T$ relation, and also have very low disc fractions ($\lesssim 0.5$) and also have large uncertainties in the disc temperature and luminosity. These are unlikely to be explained by a variation in f_{col} , and are discussed further in Section 9.

The limited low energy response of the *RXTE PCA* instrument may restrict the accurate fitting of a disc components when it does not dramatically dominate over the remainder of the continuum. The calibrated range of the *PCA* starts at around 3 keV whereas the disc temperatures peak at around $1 - 2\text{ keV}$. As we are therefore fitting only one side of the disc component, as the temperature and the luminosity fade, the slight curvature could be difficult to accurately fit especially in short observations or ones which have a small number of signal counts. Although some of the spurs could arise from weaknesses in our data analysis procedure, as they have also been seen in other studies (e.g. Gierliński & Done 2004; Done et al. 2007) it is likely that these weaknesses are not the full explanation. However Gierliński & Done (2004) only use the most disc dominated observations in their analysis. We have emulated this approach in this study when fitting lines or finding averages by selecting those observations with a very high disc fraction (> 0.8). However, the plots show all the observations which have a detected disc component. Therefore, our plots show these spurs, which may not have been shown in other studies where only the selected observations were plotted.

We also note that in a study of LMC X-3 by Steiner et al. (2010), the observations from *RXTE PCA* PCU-2 gave a very consistent value for the inner radius, a value which was also consistent with those obtained from other detectors (e.g. *Suzaku*, *Swift* and *XMM-Newton*). In our study we also find no evidence for the spurs seen in other BHXR in LMC X-3, and so their study does not help in clarifying whether the spurs come from instrumental effects. However the close correspondence of the R_{in} between *RXTE* and the other detectors does indicate that in the disc dominated state, the spectral coverage of the *PCA* is sufficient to be able to accurately determine the disc parameters.

In the theoretical $L - T$ expectation, we have used a constant value for the colour correction, $f_{\text{col}} = 1.8$ (Shimura & Takahara 1995). The departures from the $L \propto T^4$ law could be the result of the variation of the value of f_{col} . The colour correction factor accounts for the change in the dominant emission process in the inner disc, and therefore is a function of L_{Disc} . Gierliński & Done (2004) showed that the f_{col} is approximately constant throughout the outburst (see also Shimura & Takahara 1995; Merloni et al. 2000; Davis et al. 2006). However these were only for the most disc dominated observations. Therefore it is possible that f_{col} variations could have occurred in the BHXR presented in these studies, but not be shown in the figures. If f_{col} is constant during the most disc

dominated phases of the outburst, and only those phases are shown, then any variation would not be detected.

To account for these spurs, f_{col} would decrease at the beginning of the outburst, and then increase on the exit of the outburst as the BHXRb goes through the intermediate states (see the schematic in Appendix Fig. A.1). The motion off the T^4 relation is approximately perpendicular. Therefore a simple change in f_{col} would explain the deviations, without needing any further variation (of inner disc radius, for example). It is of course possible that the disc radius is not constant at the very beginnings and ends of the outburst. However, if the f_{col} is not constant then it will be difficult to determine what the true R_{in} is in these non dominant discs observed by *RXTE*.

We show on the $L - T$ plane in Appendix Fig. A.1 the theoretically expected relation for $f_{\text{col}} = 1.8$ but also for a range of values for f_{col} between 1.6 and 2.6. The lower limit arises from the initial investigation into f_{col} by Shimura & Takahara (1995), whereas the upper comes from the best characterised BHXRb in Gierliński & Done (2004). In cases where the values of the distance and mass used are such so that the theoretical $L - T$ relation is a good match to the observed $L - T$ relation, then the spurs, should they be present, mostly fall within this $1.6 < f_{\text{col}} < 2.6$ range. In Appendix Fig. A.1 we also show a schematic which indicates the route taken by a BHXRb in this diagram.

If these spurs are purely the result of changes in f_{col} , we can calculate the change in f_{col} required, δf_{col} , for the spurs to be part of the expected $L - R_{\text{in}}^2 T^4$ relation, under the assumption that the disc radius is constant. We assume that $f_{\text{col}} = 1.8$ when the T^4 relation is followed, and so adjust the normalisation of Equation 1 so that the expected relation falls under the observed points at $kT = 1$ keV. As this normalisation is affected by the distance, mass, and inclination, which in many BHXRbs are only estimates, this simplifies our approach, without affecting our conclusions on the variation of f_{col} . We also note that the spin of a black hole can affect the normalisation. We are currently assuming that the black hole is not rotating, but discuss spinning black holes in see Section 8. In Appendix Fig. A.1 we show for each BHXRb the excess f_{col} required for the observation to lie on the T^4 relation, δf_{col} , against the powerlaw and disc fractions of the observation. In most cases this centred on $\delta f_{\text{col}} = 0.0$, which is by design, though where the $L - T$ relation slope is very different from 4 (Section 5), then the position along the x -axis can vary.

There appear to be three regions in the diagrams. The observations with the largest disc fractions cluster around $\delta f_{\text{col}} = 0.0$, as defined by the normalisation adjustment mentioned above. The δf_{col} remains almost constant at zero over around an order of magnitude change in the disc fraction. These are the observations which scatter around the theoretically expected T^4 relation, as the f_{col} is constant.

As the disc fraction decreases the trend is for the observations to move gradually towards progressively higher values of f_{col} , δf_{col} increases. These are the beginnings of the spurs, but are also visible as lopsidedness in the scatter around the most disc dominated observations in the plots of L_{Disc} versus T .

At around $\delta f_{\text{col}} = 0.5$ the trend in the observations flattens off, as the disc fraction approaches zero, resulting in large changes in f_{col} over small changes in the disc fraction. These observations are the ones from the spurs and extend up to $\delta f_{\text{col}} \sim 1.0$. The value of f_{col} required for these observations to lie on the T^4 relation become larger with very little change in the disc fraction. The x -axes of the figures has been truncated as the observations with very low disc fractions which lie well below the main cluster of points have

up to $\delta f_{\text{col}} \sim 20$ (see Section 9). These observations are unlikely to be explained by a varying f_{col} and hence we do not show them in the figure.

The most recent investigation into f_{col} by Done & Davis (2008) shows that there is a positive correlation between the f_{col} and the mass accretion rate. The effect is stronger for a proportional counter array (e.g. the *RXTE PCA*) than for a Charge-Coupled Device (CCD) and shows that for an alpha disc, with $\alpha = 0.1$, f_{col} can reach values of around 2.1 for accretion rates of 10^{19} g/s (for a KERRBB disc model). This is lower than the f_{col} increase inferred in Appendix Fig. A.1, but links the accretion rate to the f_{col} . Although the evolution of the f_{col} over time indicated by Done & Davis (2008) is different, the clear link between the deviations from $L - T^4$ and f_{col} suggests a link to the accretion rate. However, it must be noted that the color correction fraction and, in general, the observed properties of the high-energy tail of the disc emission are quite sensitive to the vertical structure of the disc. In particular, as discussed in more detail in Davis et al. (2005) and Done & Davis (2008), the vertical dissipation profile may be very different in spectral states where a non-thermal (power-law) component is significantly detected, as a larger fraction of the total accretion power has to be released near or above the disc surface, leading to a possible increase in the estimated color correction factors.

Both a constant f_{col} and a constant R_{in} are observed when the disc fraction is high ($\gtrsim 0.8$), i.e. in those observations where the disc emission dominates over the powerlaw emission, and the disc parameters have been well determined. However, under the assumption of a constant f_{col} , as the disc fraction reduces the inferred R_{in} decreases, which has a knock-on effect on the behaviour of the disc temperature with the luminosity. However, the drastic nature of the decrease in the R_{in} is such, that a increase in f_{col} may be a more reasonable explanation. If the true underlying behaviour of the BHXRb is that the inner radius remains constant, then an increase of the f_{col} could account for the majority of the spurs observed.

8 DISTANCES, MASSES AND SPINS FROM DISC PARAMETERS

During the most disc dominated parts of the outburst, the inner radius of the disc and the f_{col} are approximately constant. The estimated disc parameters (temperature and luminosity) depend on the physical parameters of the BHXRb system - the distance, mass and spin of the black hole. However, these parameters are constant for a particular BHXRb. Therefore, the *shape* that the observations make in the $L - T$ plane are fixed, but their *location* within the plane could vary, depending on these parameters.

Using the theoretical relation (Equation 1) and the data we are able to place limits on the distances and masses of the BHXRbs, in the case of a Schwarzschild black hole. From Equation 1, the theoretically expected $L - T$ relation is of the form of

$$\frac{L_{\text{Disc}}}{L_{\text{Edd}}} = AMT^4, \quad (3)$$

where M is the mass of the black hole. When fitting the trend in the $L - T$ plane for the most disc dominated states, the form is (for constant R_{in} and f_{col})

$$\frac{L_{\text{Disc}}}{L_{\text{Edd}}} = B \frac{D^2}{M} T^C, \quad (4)$$

where T is the observed temperature, B is derived from the normalisation of the DISKBB component in XSPEC and D is the distance of the BHXR. The dependence on M and D in these two equations are different. As these two Equations should be equal, assuming the fitted value of $C = 4$, then

$$AM = B \frac{D^2}{M}. \quad (5)$$

However, the slope of the fits to the $L - T$ relation do not always end up with $C \sim 4$. Therefore, in order to remove this dependence we calculate the match at $kT = 1$ keV, which is close to the temperatures of the observed discs.

Therefore, under the assumption that R_{in} and f_{col} are constant, we can determine the distances and masses which are required in order that the location of the expected $L - T$ relation matches those which are observed. In cases where limits have been placed on either the distance or mass, then we are able to constrain the acceptable values for the mass or distance respectively. These loci of points in the distance-mass diagram are shown in the Appendix, Fig. A.1 by the blue line, and we also show the current best estimates on the distances and masses and their uncertainties, where they exist. In some cases (e.g. GRS J1739-278, XTE J1650-500 LMC X-1) the fitted slope is very different to 4, and so there in these cases, these loci are not reliable.

In some cases the current best observational estimates on the distances and masses do coincide with the estimates from this work (e.g. 4U 1543-47, GX 339-4, XTE J1720-318). However in many cases there is no overlap between the observed estimates on the distance and mass and those calculated here (e.g. GRO 1655-40, XTE J1550-564). Although at face value, cases where there is no overlap would allow the distance and mass estimates to be refined, it is not quite that simple. These constraints are for a non-rotating black hole, and there is significant evidence that at least some black holes have significant spin (see e.g. Miller et al. 2009; McClintock et al. 2006; Middleton et al. 2006 and also Fender et al. 2010 and references therein).

The normalisation of the theoretically expected relation between L_{Disc} and T changes when the black hole is maximally spinning ($a^* = 0.998$) (see e.g. Gierliński & Done 2004). We use a very simple parameterisation from Makishima et al. (2000) who include first order effects of the black hole spin on the theoretically expected relation in terms of

$$\alpha = R_{\text{in}}/3R_{\text{S}},$$

the ratio of the inner disc radius to the Schwarzschild radius ($\alpha = 1$ and $\alpha = 1/6$ for a non rotating and maximally rotating black hole respectively). This appears as an α^2 term in their version of Equation 1. We add this correction factor into Equation 1, and also take into account the changes in the general relativistic correction factors from Zhang et al. (1997) for rotating black holes.

Therefore, we show in Appendix, Fig A.1, as well as the range of distances and masses allowed for a non-rotating black hole, we also show those for a maximally rotating black hole ($a^* = 0.998$, red line) and one for $a^* = 0.5$ (green line). This results in an area in the $D - M$ plane in which both values are allowed. We note, that, a more accurate investigation would start with a more appropriate model for the disc emission including the relativistic effects of the black hole spin (e.g. KERRBB). We have, as yet, not re-fitted all our results with such a model. These plots show that many of the BHXRBS whose distances and masses did not match the loci for a non-rotating black hole, do match if the black hole is rotating (e.g. GRO J1655-40, XTE J1550-564, XTE J1650-500, LMC X-3). The

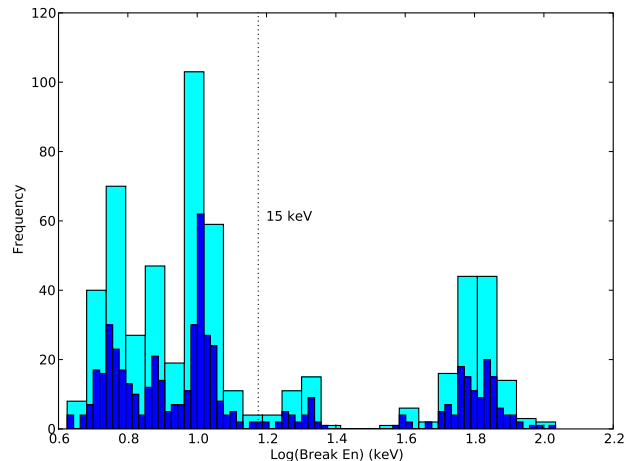


Figure 2. The distribution of the break energy for the broken power-law fits using two different binning levels. The gap between $1.4 < \log_{10} E_{\text{Break}} < 1.6$ arises from the cross over of the *PCA* and *HEXTE* instruments.

eight BHXRBS which have both mass and distance estimates, are all consistent with spin values $0 < a^* < 0.998$, or, alternatively the inner radii are consistent with $R_{\text{g}} < R_{\text{in}} < 6R_{\text{g}}$. In fact, none of the estimates on the spin of the black hole require high spin values ($a \sim 1$). This also indicates that there are no counter-rotating discs in these BHXRBS. As the estimated spins fall in the range expected for Kerr black holes, this indicates that the position of R_{in} in the disc dominated states is mainly determined by strong gravitational effects.

For many of the BHXRBS in this sample, either the mass or the distance or both are unknown. If only one is known, then limits on the other can be placed from the range allowed by the black holes spin. However, in many cases these limits are not very constraining (e.g. GRS J1739-278, XTE J1720-318). If both are unknown, then the best that can be obtained is a lower limit on the distance (assuming a reasonable lower bound for the black hole mass).

9 BROKEN POWERLAW - DISC MODEL DEGENERACY

The limitations of the spectral response of the *RXTE PCA* make the unequivocal detection of a non-dominant disc very difficult. When the disc's spectral component begins to rise above the powerlaw, the difference in the χ^2_{ν} between the broken powerlaw and disc + powerlaw model is very small. It is therefore difficult to say *ab initio* which of the two models is the most appropriate to select for the observation (see Dunn et al. 2010). In our selection procedure we select merely on the lowest reduced χ^2 , with some restrictions on the model parameters. We now investigate how adapting the model selection procedure affects the numbers and parameters of the discs detected.

As the broken powerlaw model could mimic a disc model, especially when the break energy is low ($\lesssim 10$ keV). We show in Fig. 2 the distribution of the break energies in the observations best fit by the broken powerlaw model, using two different binning schemes. The gap around $\log_{10} E_{\text{break}} = 1.4$ is the result of the crossover between the *PCA* and the *HEXTE* instruments at 25 keV.

The main cluster of points occur at low energies, with another smaller cluster at around $\log_{10} E_{\text{break}} = 1.8$. These observations with high break energies ($E_{\text{break}} \sim 60$ keV) are likely to be re-

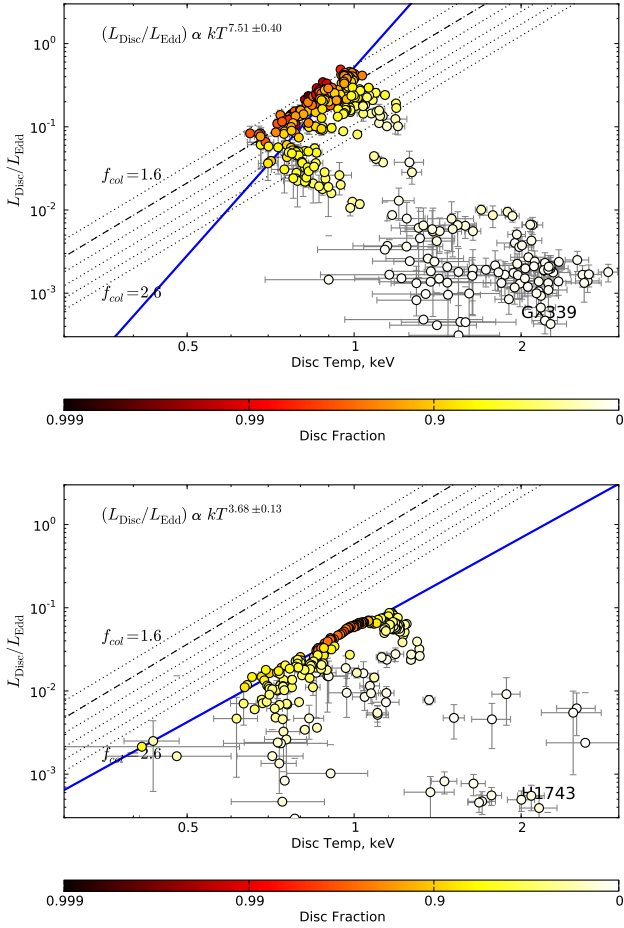


Figure 3. The variation of the disc luminosity with the disc temperature for GX 339-4 and H 1743-322 when penalising the χ^2 of broken powerlaw models which have a break energy < 15 keV. For comparison plots see Appendix Fig. A.1.

liable fits to a true break in the spectrum. However, those which fall below around $E_{\text{break}} \sim 10$ keV could be the result of a non-dominant disc mimicking a broken powerlaw

We redo the model selection procedure but penalise the broken powerlaw models where the break energy is lower than 15 keV. In some cases only one of the two powerlaw fits (with and without line) has a break energy < 15 keV, and then the remaining broken powerlaw fit is still allowed. However, this only occurs in rare cases. The other two remaining options are then single powerlaw or disc+powerlaw models (each with and without a line). We expect that this will have most effect in the intermediate states, where non-dominant discs are expected, rather than in the most disc dominated states where $L \propto T^4$.

In Fig. 3 we show the $L - T$ plane for GX 339-4 and H 1743-322 as an example to show the increase in the number of observations which have a low disc fraction. These extra observations appear below the T^4 relation, and the spurs appear to merge in with them. Most of these observations have large uncertainties in both the disc temperature and luminosity.

Doing the converse on the selection procedure - favouring the broken powerlaw models in these situations - removes most of the observations with a disc detection at very low disc fractions (lower right in the $L - T$ plane) in Appendix Fig. A.1. Although this is

may be a more conservative selection procedure (no discs detected when they may be uncertain), it is less informative on the behaviour of the BHXRBS on the transitions between the different states.

It is therefore difficult to determine what the appropriate selection procedure is when broken powerlaw and disc models are both good fits to the data. The spectral resolution and low energy range of the *RXTE PCA* are very limiting in this case. Future investigations or instruments may aid in pin-pointing the disc behaviour in the transition regions

10 POWERLAW EVOLUTION

Using the Disc Fraction Luminosity Diagram (DFLD) to investigate the behaviour of a BHXRBS during an outburst restricts what information can be extracted about the variation of the powerlaw component, especially in the hard/powerlaw-dominated state. In this state, the variation in the powerlaw slope or break energy do not effect the disc fraction, and so all observations fall on a single line.

In Appendix Fig. A.2 we show the DFLDs for the X-ray binary in question, where the colour scale shows the variation of the powerlaw slope (below the break if it is a broken powerlaw). We show in the neighbouring panel, the powerlaw slope against the total luminosity for those observations with a disc fraction of < 0.2 (powerlaw fraction > 0.8). This allows the change in the powerlaw slope to be tracked in the powerlaw dominated state. In a number of binaries there are insufficient observations in the hard state to determine any trend with time. Also, 4U 1630-47, the variation of the powerlaw slope appears complex, with no easily discernable global trend. However, the outburst structure in this BHXRBS is also complex and so this variation is expected (see Dunn et al. 2010).

In the majority of BHXRBS, in the low luminosity “stalk”, the powerlaw slope increases as the luminosity falls – the spectrum softens. This has been seen in the HIDs of the BHXRBS before, as a change in the X-ray colour. The re-emergence of the disc at very low luminosities has been observed in deep pointed observations and may also play a role in the softening of the spectrum at low luminosities (see Cabanac et al. 2009). However, at these low luminosities the effects of the Galactic Ridge Emission (GRE) play a role. None of the BHXRBS were fitted with a model which takes into account the effects of the GRE in their vicinity (Dunn et al. 2010). At low luminosities, the GRE can have an appreciable effect on the shape and flux of the spectrum. However, the curvature in the stalk was seen in the study of GX 339-4 by Dunn et al. (2008), where the GRE was added to the model spectrum as a fixed component. Therefore only part of the softening at low luminosities can be explained by the GRE.

However, at the top of the powerlaw dominated state in some BHXRBS, there is an increase in the powerlaw slope. The increase in Γ has been observed as the BHXRBS enters the soft or disc-dominated state. However, in these Figures, the Γ increases far beyond what has been observed in other studies of these BHXRBS, using the same data (e.g. Motta et al. 2009). The likeliest explanation is that the broken powerlaw is accounting for a rising disc, which is not being well fit by a disc model. What can also be seen is that these softer powerlaw slopes are from broken powerlaws, and they have a comparatively low break energy. As noted in Dunn et al. (2010) and Section 9 there is a possibility for the broken powerlaw to mimic the disc (and powerlaw) model. It is probable that as the disc rises in luminosity the limited spectral range of the *RXTE PCA* means that the curvature of the disc cannot be determined, and the

broken powerlaw resulted being a better fit. Restricting the powerlaw break to being above the peak mentioned in Section 9 would prevent this occurring. However, the accuracy of the fitted disc parameters is not clear. Therefore, the softening of the powerlaw on the transitions to the disc-dominated state is likely to be the result of the limitations of the *RXTE PCA*.

11 SUMMARY

We have investigated the behaviour of the disc and powerlaw components in the 25 BHRXBs presented in Dunn et al. (2010). In the majority of BHRXBs in which at least most of an outburst has been observed, the disc luminosity scales close to T^4 in the most disc dominated observations. This behaviour had been seen in other studies (e.g. Gierliński & Done 2004). The scaling of T^4 implies that both the disc's inner radius, R_{in} and the colour correction factor, f_{col} are relatively constant in the most disc dominated states. A number of BHRXBs do not show a clear T^4 relation, but these could be the result of the limitations of the model fitting routine or the frequency of observations.

However, in observations where the disc is no longer overly dominant, there are deviations from the T^4 law. If interpreted as changes in the disc's inner radius, these deviations imply that the disc is moving inwards at the end of an outburst, and outwards at the beginning of the outburst. Although we do not rule this behaviour out, it seems an unlikely scenario. If these deviations are attributed to changes in the colour correction factor, then f_{col} rises as the disc fraction decreases.

There are a number of observations in which the disc parameters determined are unlikely to be explained by reasonable values for the disc radius or the f_{col} . The spectral fits for these observations tend to have χ^2 values which are very similar to those for the broken-powerlaw model, which makes selecting the most appropriate model difficult. This also makes determining the true behaviour of the disc temperature, radius and f_{col} in these intermediate states difficult.

The luminosity of the disc in Eddington units can be calculated from theoretical arguments from the BHRXB parameters and the disc temperature. When calculating the observed luminosity the distance of the BHRXB system also enters the calculation. The combination of these two calculations allows the ratio of D/M to be estimated from the $L - T$ relation of the BHRXB disc. We have therefore placed limits on the range values of D and M values allowed for different values of the spin of the black hole.

ACKNOWLEDGEMENTS

We thank the referee for a prompt and useful report which helped improve the manuscript. RJHD acknowledges support from the Alexander von Humboldt Foundation. EK acknowledges financial support by a Marie Curie Reintegration Grant under contract number PERG05-GA-2009-243869. TMB acknowledges support ASI via contract I/088/06/0 and thanks the International Space Science Institute (ISSI). The research leading to these results has received funding from the European Community's Seventh Framework Programme (FP7/2007-2013) under grant agreement number ITN 215212 Black Hole Universe. This research was supported by the DFG cluster of excellence Origin and Structure of the Universe (www.universe-cluster.de).

REFERENCES

- Abramowicz M. A., Czerny B., Lasota J. P., Szuszkiewicz E., 1988, *ApJ*, 332, 646
- Augusteijn T., Kuulkers E., van Kerkwijk M. H., 2001, *A&A*, 375, 447
- Belloni T. M., 2010, in *Lecture Notes in Physics*, Berlin Springer Verlag, Vol. 794, *Lecture Notes in Physics*, Berlin Springer Verlag, T. Belloni, ed., pp. 53–+
- Cabanac C., Fender R. P., Dunn R. J. H., Körding E. G., 2009, *MNRAS*, 396, 1415
- Cadolle Bel M., Rodriguez J., Sizun P., Farinelli R., Del Santo M., Goldwurm A., Goldoni P., Corbel S., Parmar A. N., Kuulkers E., Ubertini P., Capitanio F., Roques J.-P., Frontera F., Amati L., Westergaard N. J., 2004, *A&A*, 426, 659
- Campana S., Stella L., Belloni T., Israel G. L., Santangelo A., Frontera F., Orlandini M., Dal Fiume D., 2002, *A&A*, 384, 163
- Capitanio F., Ubertini P., Bazzano A., Kretschmar P., Zdziarski A. A., Joinet A., Barlow E. J., Bird A. J., Dean A. J., Jourdain E., De Cesare G., Del Santo M., Natalucci L., Cadolle Bel M., Goldwurm A., 2005, *ApJ*, 622, 503
- Casares J., Zurita C., Shahbaz T., Charles P. A., Fender R. P., 2004, *ApJ*, 613, L133
- Chaty S., Haswell C. A., Malzac J., Hynes R. I., Shrader C. R., Cui W., 2003, *MNRAS*, 346, 689
- Corbel S., Fender R. P., Tzioumis A. K., Nowak M., McIntyre V., Durouchoux P., Sood R., 2000, *A&A*, 359, 251
- Corbel S., Nowak M. A., Fender R. P., Tzioumis A. K., Markoff S., 2003, *A&A*, 400, 1007
- Cowley A. P., Crampton D., Hutchings J. B., Remillard R., Penfold J. E., 1983, *ApJ*, 272, 118
- Cui W., Heindl W. A., Swank J. H., Smith D. M., Morgan E. H., Remillard R., Marshall F. E., 1997, *ApJ*, 487, L73+
- Davis S. W., Blaes O. M., Hubeny I., Turner N. J., 2005, *ApJ*, 621, 372
- Davis S. W., Done C., Blaes O. M., 2006, *ApJ*, 647, 525
- di Benedetto G. P., 1997, *ApJ*, 486, 60
- Done C., Davis S. W., 2008, *ApJ*, 683, 389
- Done C., Gierliński M., 2003, *MNRAS*, 342, 1041
- Done C., Gierliński M., Kubota A., 2007, *AAAR*, 15, 1
- Dunn R. J. H., Fender R. P., Körding E. G., Belloni T., Cabanac C., 2010, *MNRAS*, 403, 61
- Dunn R. J. H., Fender R. P., Körding E. G., Cabanac C., Belloni T., 2008, *MNRAS*, 387, 545
- Fender R., Gallo E., Russell D., 2010, *ArXiv e-prints*
- Fender R. P., Belloni T. M., Gallo E., 2004, *MNRAS*, 355, 1105
- Foellmi C., 2009, *New Astronomy*, 14, 674
- Fragos T., Tremmel M., Rantsiou E., Belczynski K., 2010, *ApJ*, 719, L79
- Gelino D. M., Balman Ş., Kızıloğlu Ü., Yılmaz A., Kalemci E., Tomsick J. A., 2006, *ApJ*, 642, 438
- Gierliński M., Done C., 2003, *MNRAS*, 342, 1083
- , 2004, *MNRAS*, 347, 885
- Gierliński M., Maciołek-Niedźwiecki A., Ebisawa K., 2001, *MNRAS*, 325, 1253
- Gierliński M., Zdziarski A. A., Poutanen J., Coppi P. S., Ebisawa K., Johnson W. N., 1999, *MNRAS*, 309, 496
- Greiner J., Dennerl K., Predehl P., 1996, *A&A*, 314, L21
- Haardt F., Galli M. R., Treves A., Chiappetti L., Dal Fiume D., Corongiu A., Belloni T., Frontera F., Kuulkers E., Stella L., 2001, *ApJS*, 133, 187
- Hjellming R. M., Rupen M. P., 1995, *Nature*, 375, 464

- Hjellming R. M., Rupen M. P., Mioduszewski A. J., Smith D. A., Harmon B. A., Waltman E. B., Ghigo F. D., Pooley G. G., 1998, in *Bulletin of the American Astronomical Society*, Vol. 30, *Bulletin of the American Astronomical Society*, pp. 1405–+
- Homan J., Belloni T., 2005, *APSS*, 300, 107
- Homan J., Wijnands R., Kong A., Miller J. M., Rossi S., Belloni T., Lewin W. H. G., 2006, *MNRAS*, 366, 235
- Hutchings J. B., Crampton D., Cowley A. P., Bianchi L., Thompson I. B., 1987, *AJ*, 94, 340
- Hutchings J. B., Winter K., Cowley A. P., Schmidtke P. C., Crampton D., 2003, *AJ*, 126, 2368
- Hynes R. I., Haswell C. A., Chaty S., Shrader C. R., Cui W., 2002, *MNRAS*, 331, 169
- Hynes R. I., Haswell C. A., Shrader C. R., Chen W., Horne K., Harlaftis E. T., O’Brien K., Hellier C., Fender R. P., 1998, *MNRAS*, 300, 64
- Hynes R. I., Steeghs D., Casares J., Charles P. A., O’Brien K., 2003, *ApJ*, 583, L95
- Ichimaru S., 1977, *ApJ*, 214, 840
- in’t Zand J. J. M., Kuulkers E., Bazzano A., Cornelisse R., Cocchi M., Heise J., Muller J. M., Natalucci L., Smith M. J. S., Ubertini P., 2000, *A&A*, 357, 520
- in’t Zand J. J. M., Markwardt C. B., Bazzano A., Cocchi M., Cornelisse R., Heise J., Kuulkers E., Natalucci L., Santos-Lleo M., Swank J., Ubertini P., 2002, *A&A*, 390, 597
- Jonker P. G., Nelemans G., 2004, *MNRAS*, 354, 355
- Kitamoto S., Tsunemi H., Pedersen H., Ilovaisky S. A., van der Klis M., 1990, *ApJ*, 361, 590
- K rding E. G., Jester S., Fender R., 2006, *MNRAS*, 372, 1366
- Kotani T., Kawai N., Nagase F., Namiki M., Sakano M., Takeshima T., Ueda Y., Yamaoka K., Hjellming R. M., 2000, *ApJ*, 543, L133
- Maccarone T. J., 2002, *MNRAS*, 336, 1371
- Makishima K., Kubota A., Mizuno T., Ohnishi T., Tashiro M., Aruga Y., Asai K., Dotani T., Mitsuda K., Ueda Y., Uno S., Yamaoka K., Ebisawa K., Kohmura Y., Okada K., 2000, *ApJ*, 535, 632
- McClintock J. E., Shafee R., Narayan R., Remillard R. A., Davis S. W., Li L., 2006, *ApJ*, 652, 518
- Merloni A., Fabian A. C., Ross R. R., 2000, *MNRAS*, 313, 193
- Middleton M., Done C., Gierliński M., Davis S. W., 2006, *MNRAS*, 373, 1004
- Miller J. M., Fabian A. C., Reynolds C. S., Nowak M. A., Homan J., Freyberg M. J., Ehle M., Belloni T., Wijnands R., van der Klis M., Charles P. A., Lewin W. H. G., 2004, *ApJ*, 606, L131
- Miller J. M., Reynolds C. S., Fabian A. C., Miniutti G., Gallo L. C., 2009, *ApJ*, 697, 900
- Miniutti G., Fabian A. C., Miller J. M., 2004, *MNRAS*, 351, 466
- Motta S., Belloni T., Homan J., 2009, *MNRAS*, 400, 1603
- Narayan R., Yi I., 1994, *ApJ*, 428, L13
- Nowak M., Juett A., Homan J., Yao Y., Wilms J., Schulz N., Canizares C., 2008, in *AAS-High Energy Astrophysics Division*, Vol. 10, *AAS-High Energy Astrophysics Division*, pp. 14.04–
- Orosz J. A., Kuulkers E., van der Klis M., McClintock J. E., Garcia M. R., Callanan P. J., Bailyn C. D., Jain R. K., Remillard R. A., 2001, *ApJ*, 555, 489
- Orosz J. A., McClintock J. E., Remillard R. A., Corbel S., 2004, *ApJ*, 616, 376
- Orosz J. A., Polisenky E. J., Bailyn C. D., Tourtellotte S. W., McClintock J. E., Remillard R. A., 2002, in *Bulletin of the American Astronomical Society*, Vol. 34, *Bulletin of the American Astronomical Society*, pp. 1124–+
- Orosz J. A., Steeghs D., McClintock J. E., Torres M. A. P., Bochkov I., Gou L., Narayan R., Blaschak M., Levine A. M., Remillard R. A., Bailyn C. D., Dwyer M. M., Buxton M., 2008, *astro-ph/0810.3447*
- Park S. Q., Miller J. M., McClintock J. E., Remillard R. A., Orosz J. A., Shrader C. R., Hunstead R. W., Campbell-Wilson D., Ishwara-Chandra C. H., Rao A. P., Rupen M. P., 2004, *ApJ*, 610, 378
- Pottschmidt K., Chernyakova M., Zdziarski A. A., Lubiński P., Smith D. M., Bezayiff N., 2006, *A&A*, 452, 285
- Remillard R. A., McClintock J. E., 2006, *ARA&A*, 44, 49
- Revnivtsev M., Gilfanov M., Churazov E., 1998, *A&A*, 339, 483
- Ritter H., Kolb U., 2003, *A&A*, 404, 301
- Russell D. M., Maitra D., Dunn R. J. H., Markoff S., 2010, *MNRAS*, 620
- Sala G., Greiner J., Ajello M., Bottacini E., Haberl F., 2007, *A&A*, 473, 561
- Sanchez-Fernandez C., Zurita C., Casares J., Castro-Tirado A. J., Bond I., Brandt S., Lund N., 2002, *IAU Circ.*, 7989, 1
- Shahbaz T., Smale A. P., Naylor T., Charles P. A., van Paradijs J., Hassall B. J. M., Callanan P., 1996, *MNRAS*, 282, 1437
- Shahbaz T., van der Hooft F., Casares J., Charles P. A., van Paradijs J., 1999, *MNRAS*, 306, 89
- Shakura N. I., Sunyaev R. A., 1973, *A&A*, 24, 337
- Shimura T., Takahara F., 1995, *ApJ*, 445, 780
- Smith D. M., Heindl W. A., Swank J. H., 2002, *ApJ*, 578, L129
- Steiner J. F., McClintock J. E., Remillard R. A., Gou L., Yamada S., Narayan R., 2010, *ApJ*, 718, L117
- Thorstensen J. R., 1987, *ApJ*, 312, 739
- Tomsick J. A., Corbel S., Goldwurm A., Kaaret P., 2005, *ApJ*, 630, 413
- van der Hooft F., Heemskerck M. H. M., Alberts F., van Paradijs J., 1998, *A&A*, 329, 538
- Wagner R. M., Foltz C. B., Shahbaz T., Casares J., Charles P. A., Starrfield S. G., Hewett P., 2001, *ApJ*, 556, 42
- Wilson C. A., Patel S. K., Kouveliotou C., Jonker P. G., van der Klis M., Lewin W. H. G., Belloni T., M endez M., 2003, *ApJ*, 596, 1220
- Zdziarski A. A., Gierliński M., Mikołajewska J., Wardziński G., Smith D. M., Harmon B. A., Kitamoto S., 2004, *MNRAS*, 351, 791
- Zhang S. N., Cui W., Chen W., 1997, *ApJ*, 482, L155+

APPENDIX

For each BHXR B in our sample we show in Fig. A.1 TOP LEFT the disc temperature as a function of the disc luminosity, along with the theoretically expected relation for the case that the BH is not rotating for a variety of values for f_{col} . The $f_{\text{col}} = 1.8$ line is depicted thicker than the rest, which increment in 0.2 intervals. The line which best fits the most disc dominated spectra is shown, as well as its slope. We show TOP RIGHT the region in the distance-mass plane which is allowed by the theoretical expectation of the luminosity-temperature relation and the observed data points. The best determined values for the distance and mass along with their uncertainties are also shown where available.

In the BOTTOM LEFT we show the variation of the disc radius (R_{in}) with the disc temperature. The colourscale is the disc fraction. The line is the average of the disc radii for the observations which have a disc fraction > 0.8 . The variation of the f_{col} with the

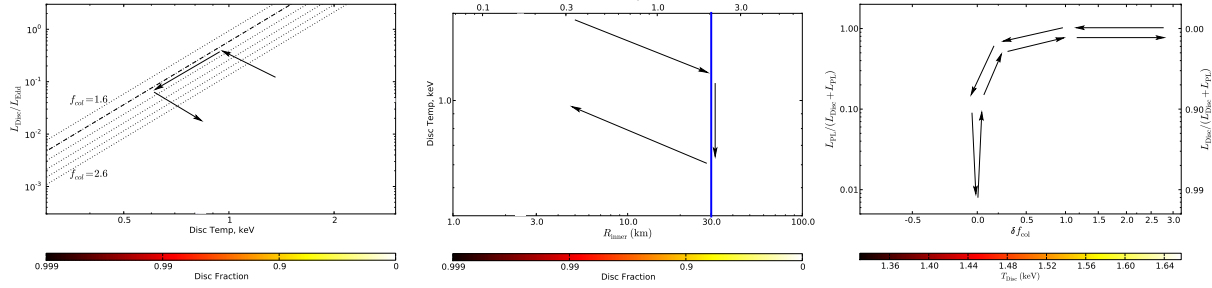


Figure A.1. Schematic figures of LEFT: Disc luminosity against disc temperature, MIDDLE: Disc radius against disc temperature and RIGHT: the excess δf_{col} required against the disc fraction. The arrows show the motion through the diagram. In the right-hand figure, the offset between the inward and outward tracks are for clarity only.

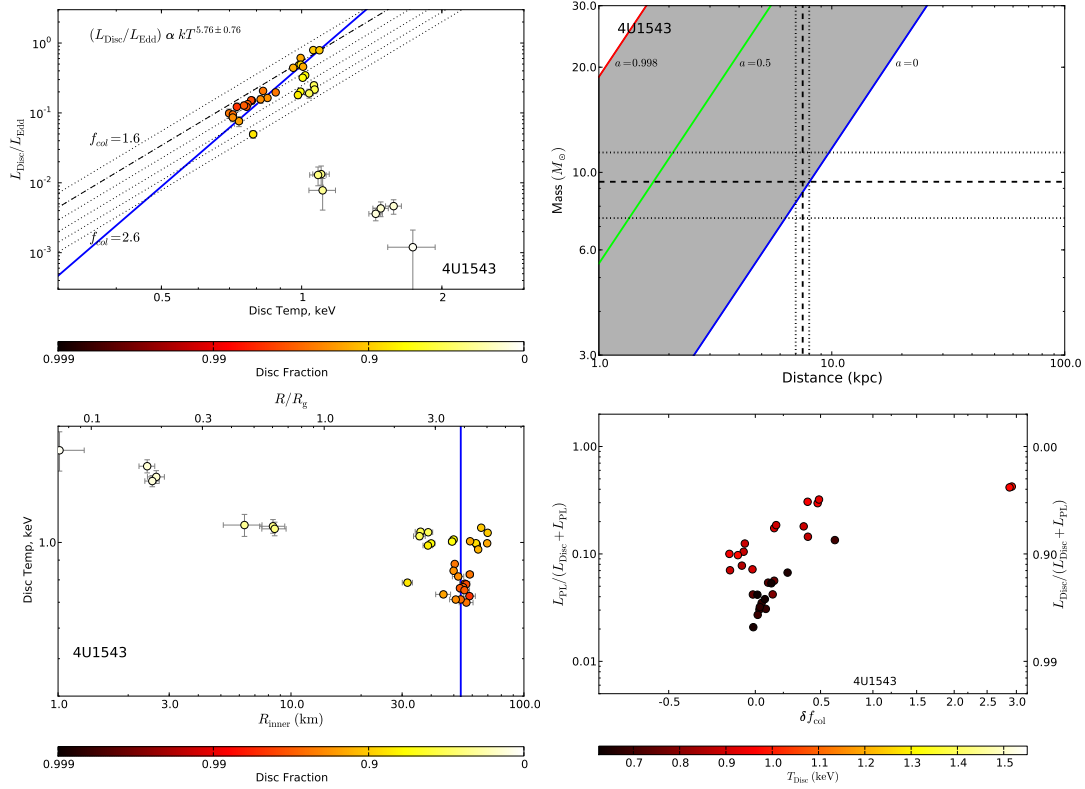


Figure A.1. (cont) 4U 1543-47 TOP LEFT We show the Luminosity of the disc as a function of the temperature of the DISCBB component in XSPEC. The colour scale is the disc fraction of the observation. The theoretical $L - T$ relations are shown by the sets of dotted line for a number of values of f_{col} . The solid line shows the fit to the most disc dominated states (Disc Fraction > 0.8). TOP RIGHT We show the range of distances and masses allowed, if the observations are to match the theoretical relation. The blue line is for a non-rotating black hole, and the direction for increasing α is shown. The dashed and dotted lines show the current values and uncertainties on the masses and distances where available. BOTTOM LEFT We show the variation of the inner disc radius (R_{in}) with the disc temperature. The colour scale is the disc fraction of the observation. The solid line shows the average R_{in} of the most disc dominated states (Disc Fraction > 0.8). BOTTOM RIGHT The excess the colour correction required, δf_{col} , with the disc fraction. The disc temperature is the colour scale.

disc fraction is show in the BOTTOM RIGHT. The disc temperature is the colour scale.

By comparing all three of the scatter plot figures, the behaviour of the disc in the BHXRB in the outburst becomes clearer.

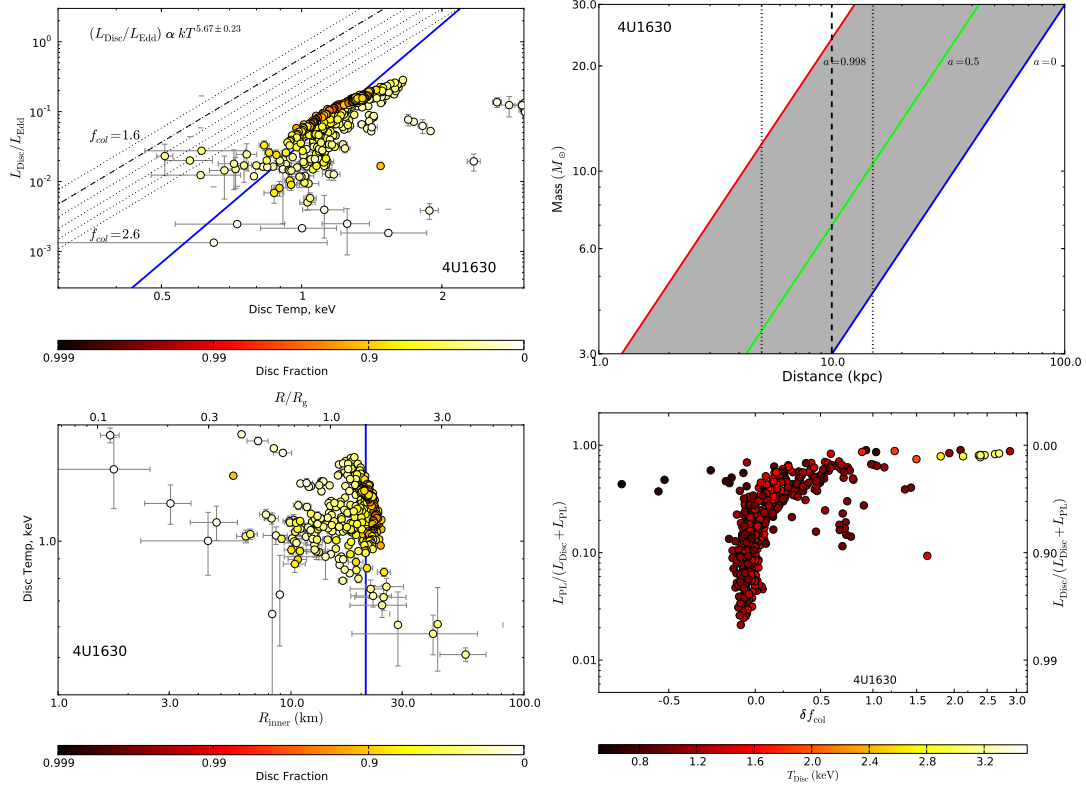


Figure A.1. (cont) 4U 1630-47

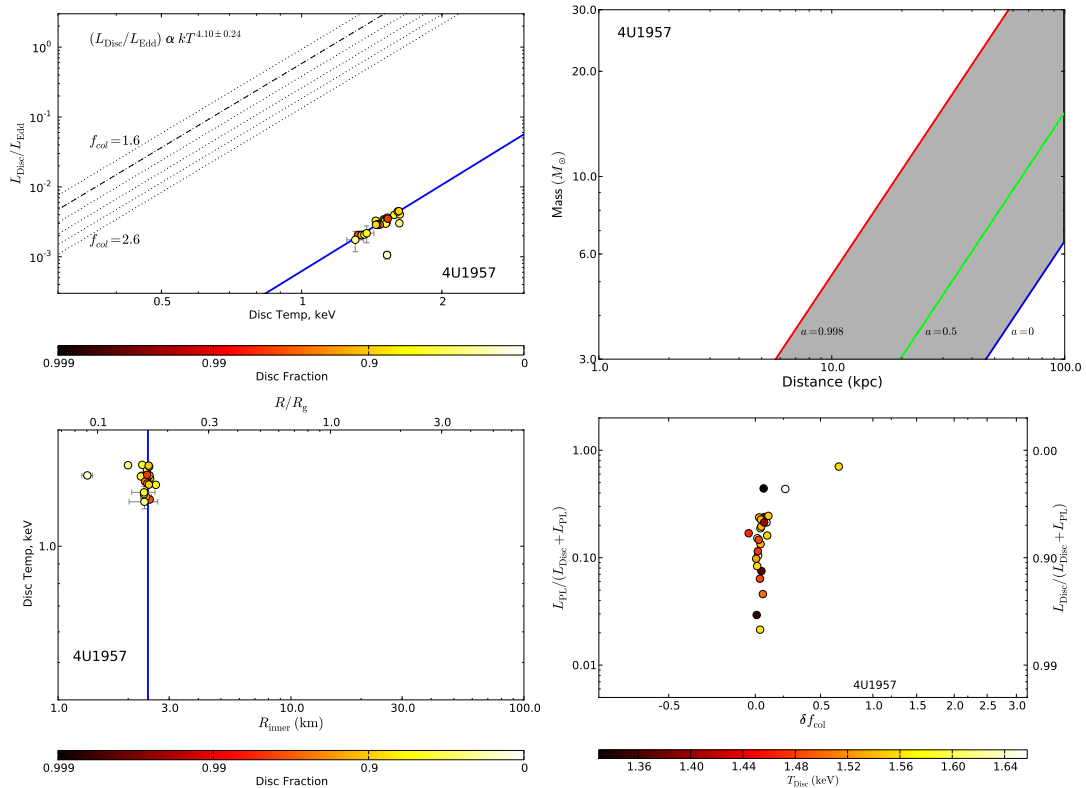


Figure A.1. (cont) 4U 1957+115

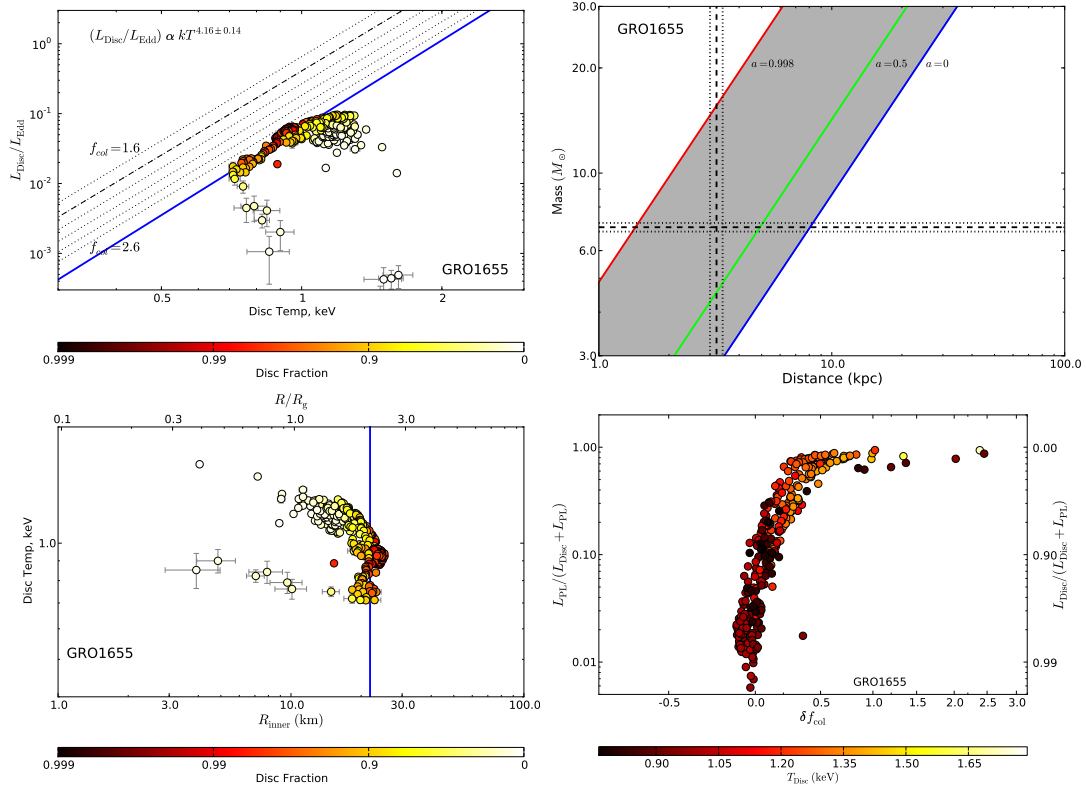


Figure A.1. (cont) GRO J1655-40

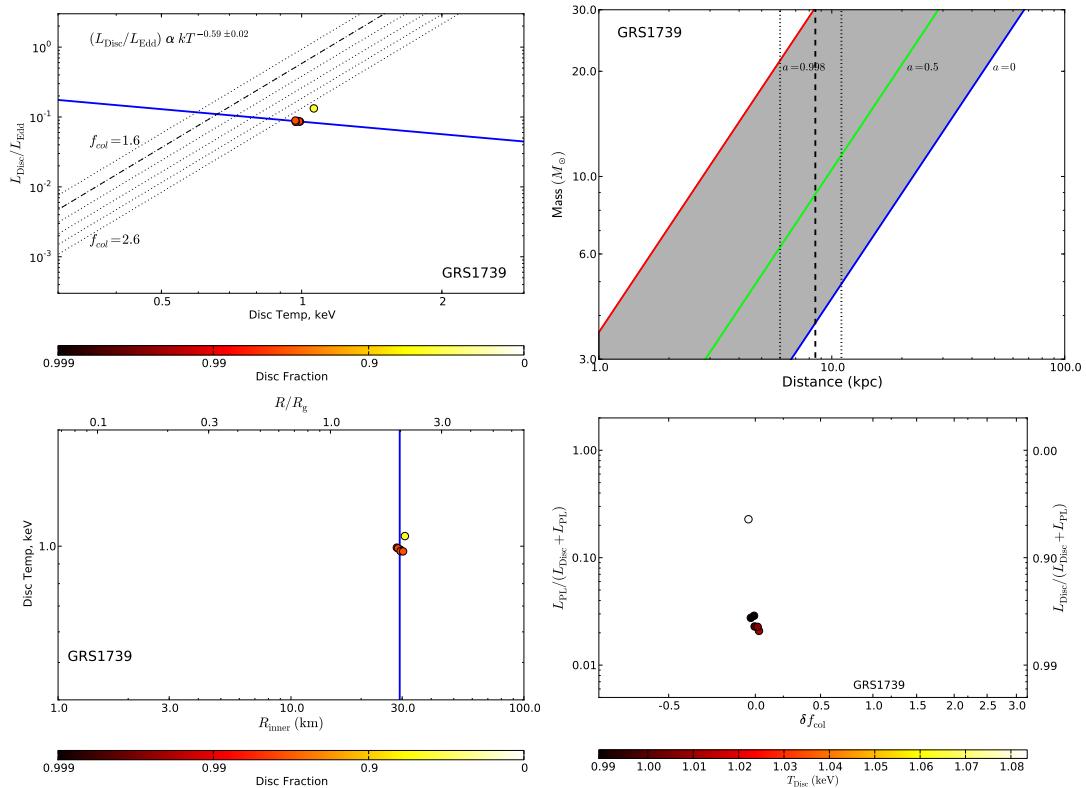


Figure A.1. (cont) GRS 1737-31

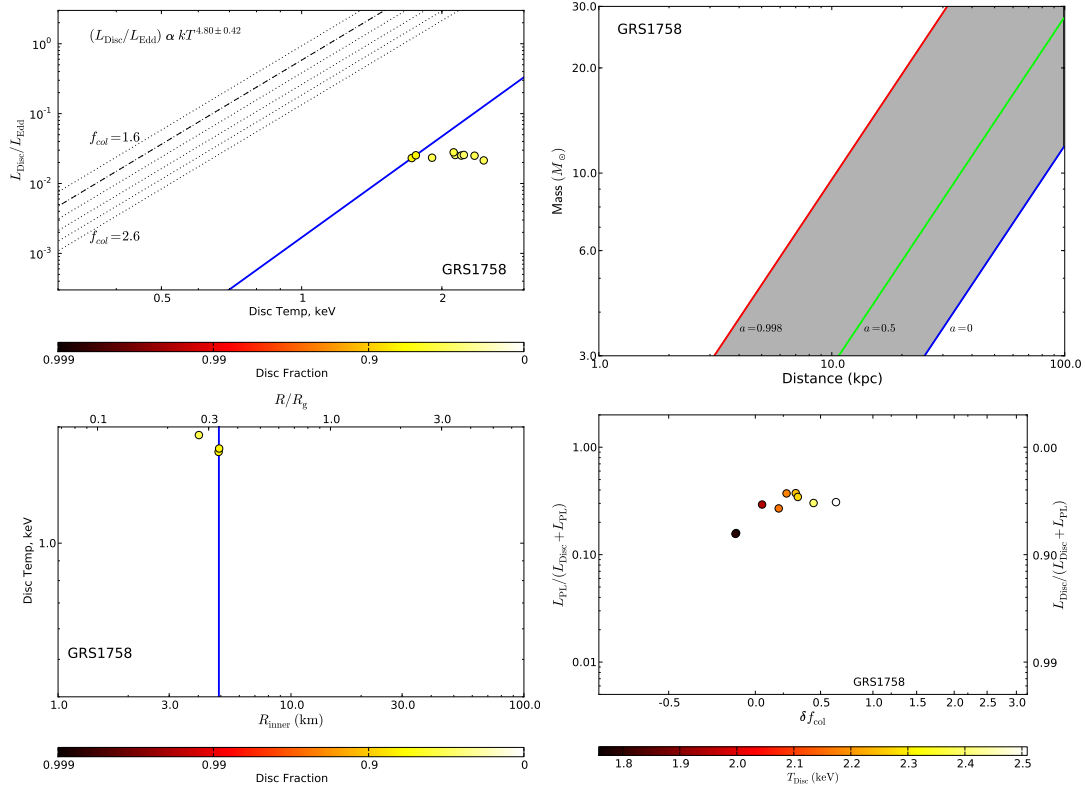


Figure A.1. (cont) GRS 1758-258

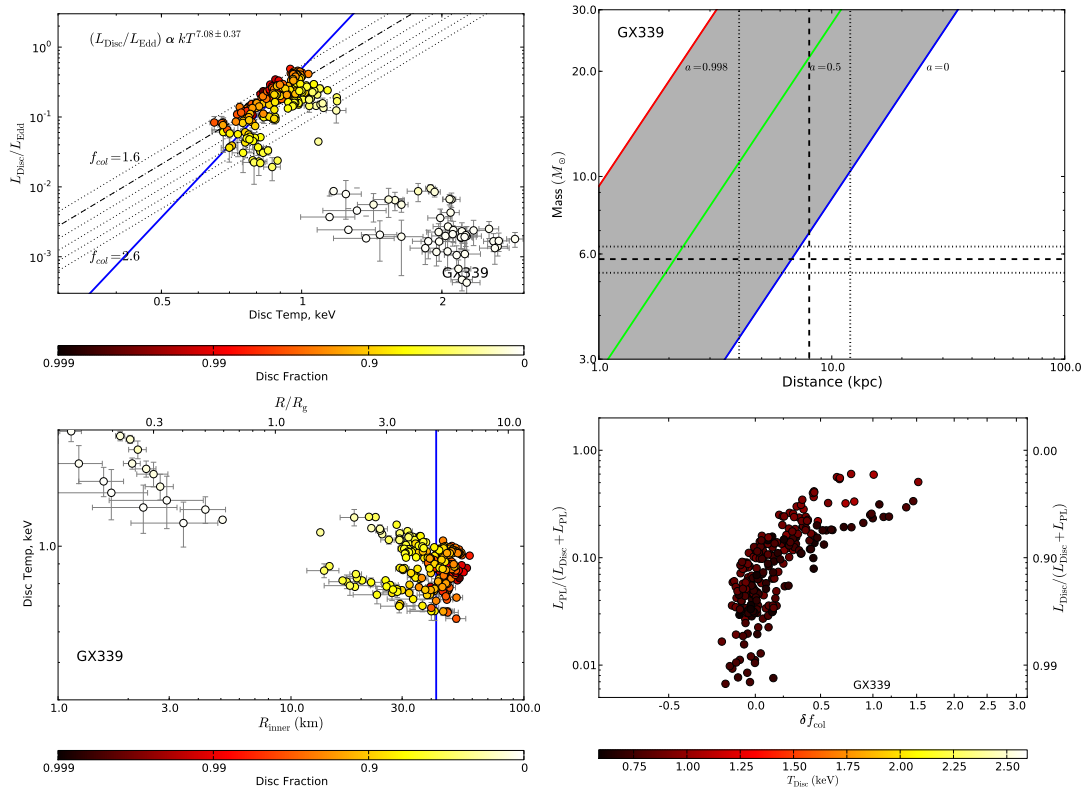


Figure A.1. (cont) GX 339-4

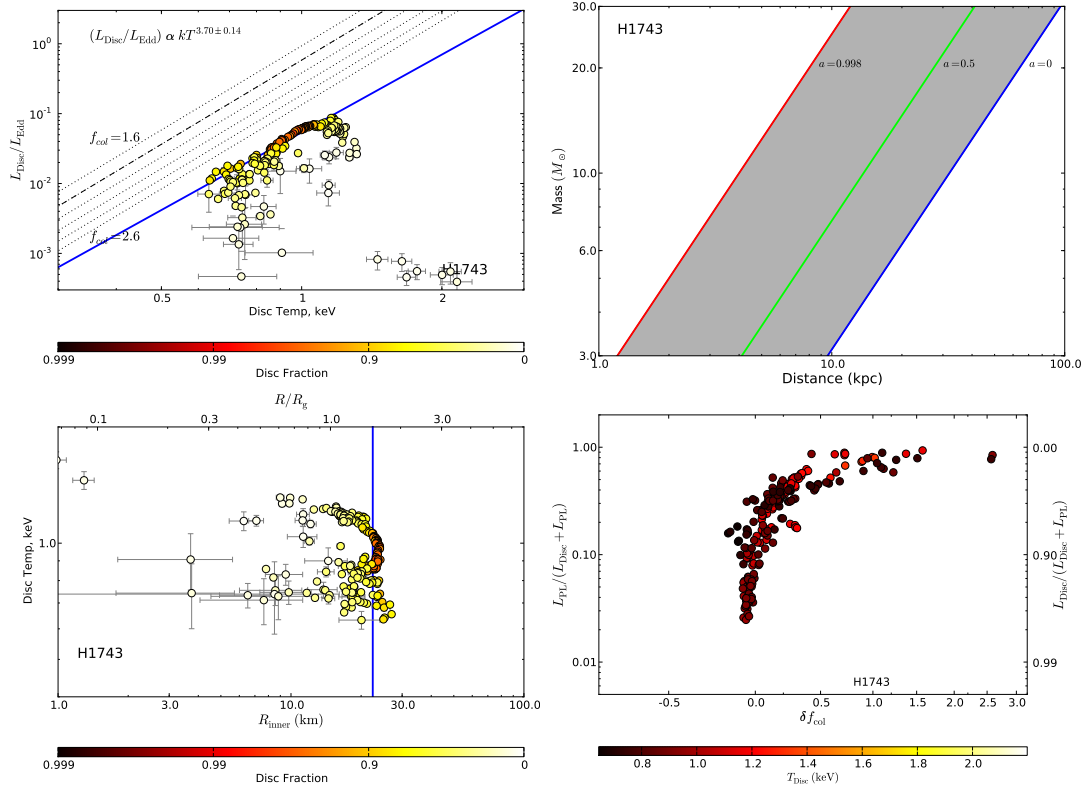


Figure A.1. (cont) H 1743-322

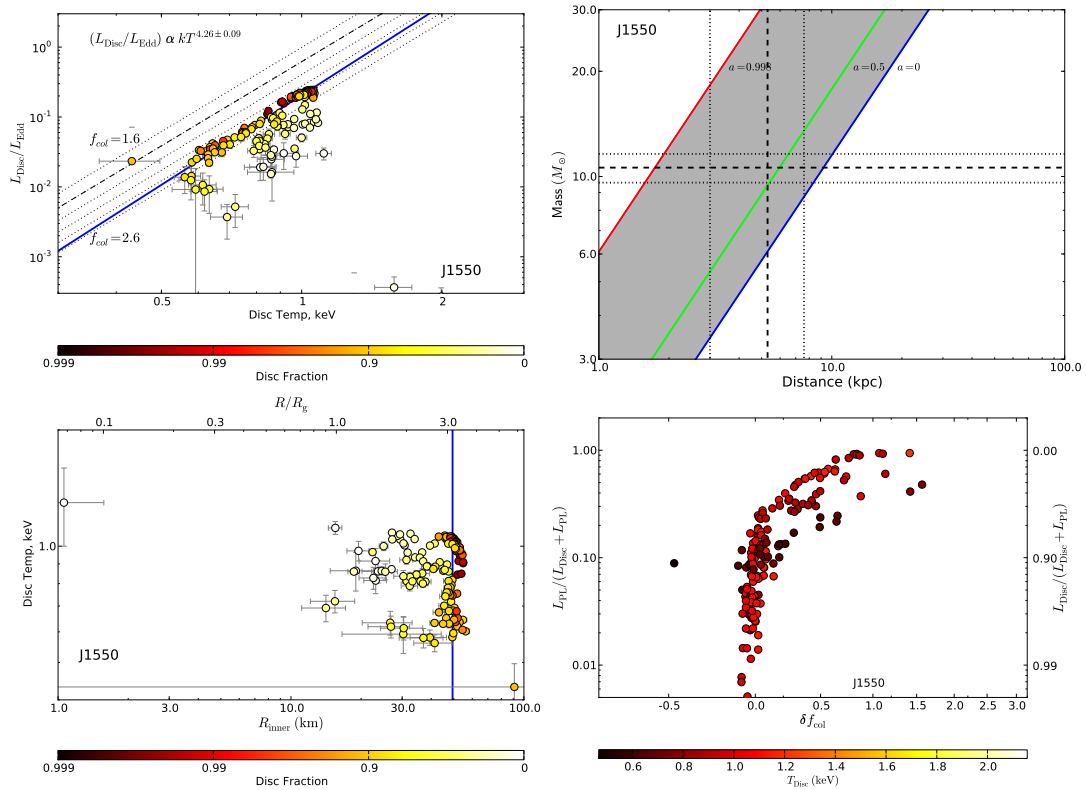


Figure A.1. (cont) XTE J1550-564

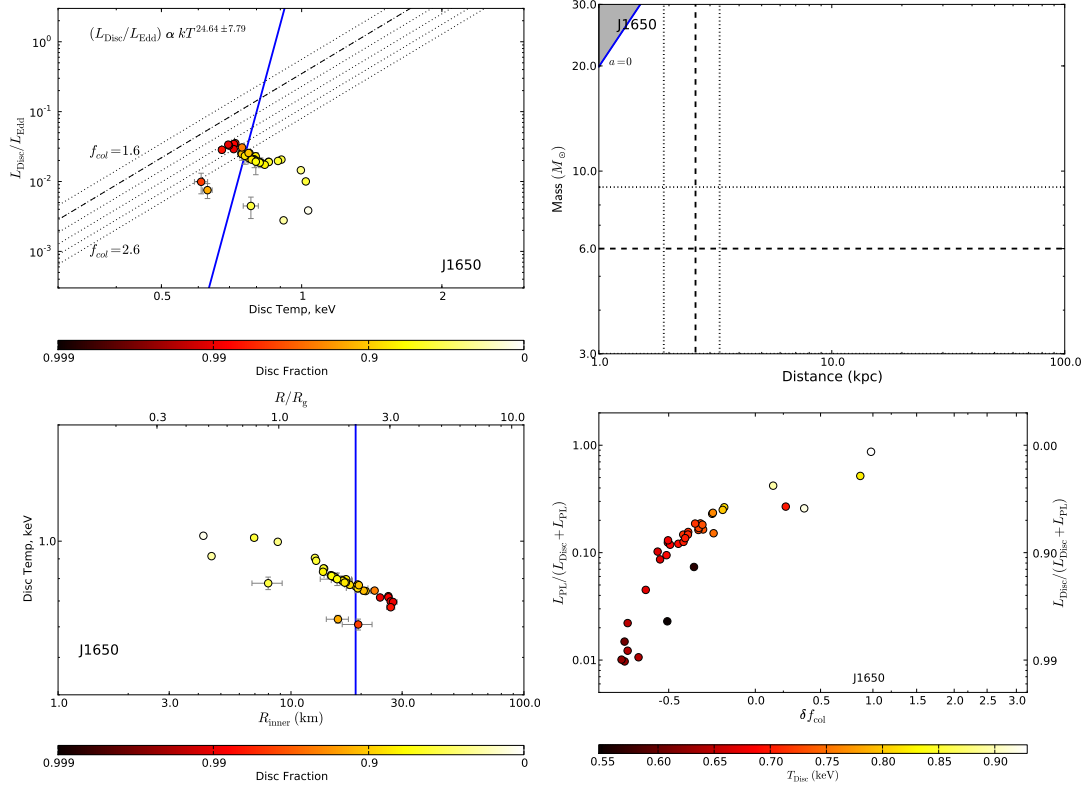


Figure A.1. (cont) XTE J1650-500

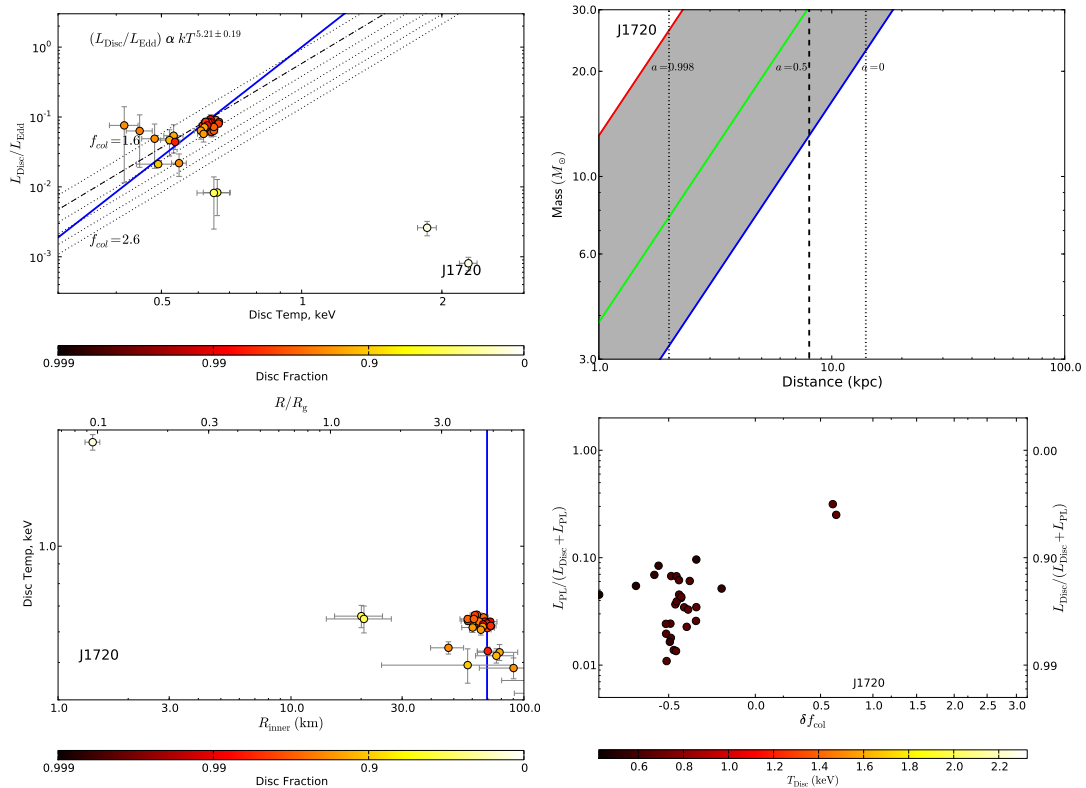


Figure A.1. (cont) XTE J1720-318

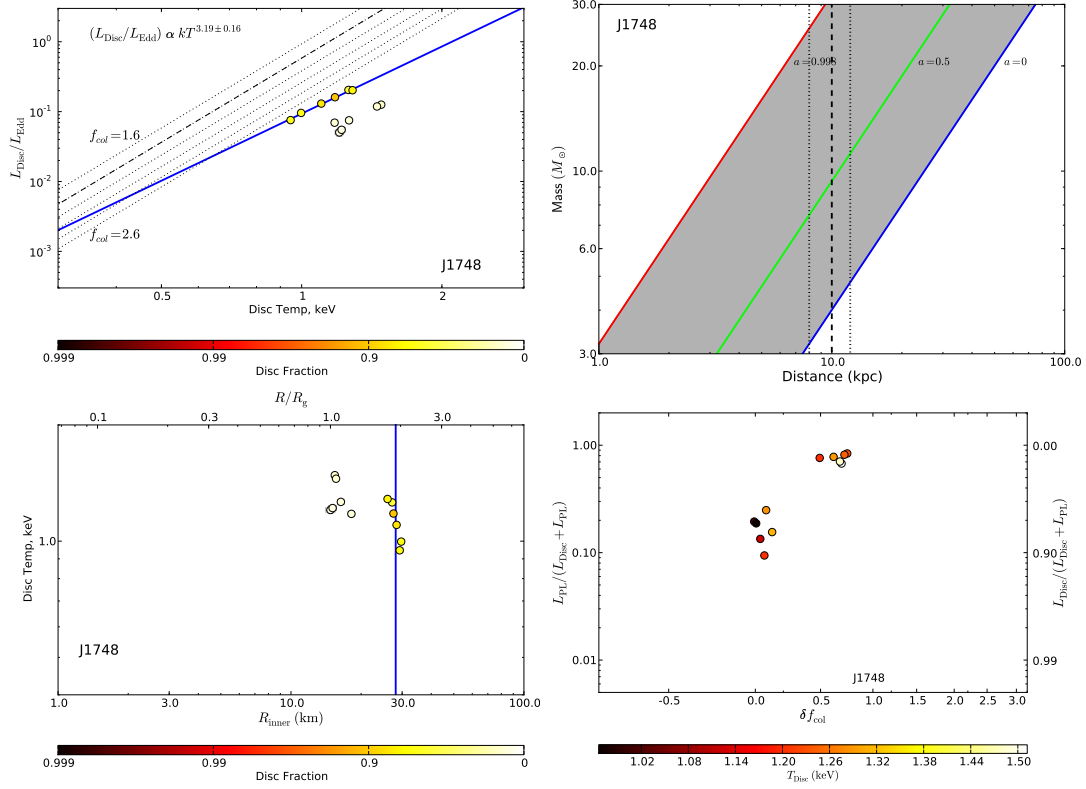


Figure A.1. (cont) XT J1748-288

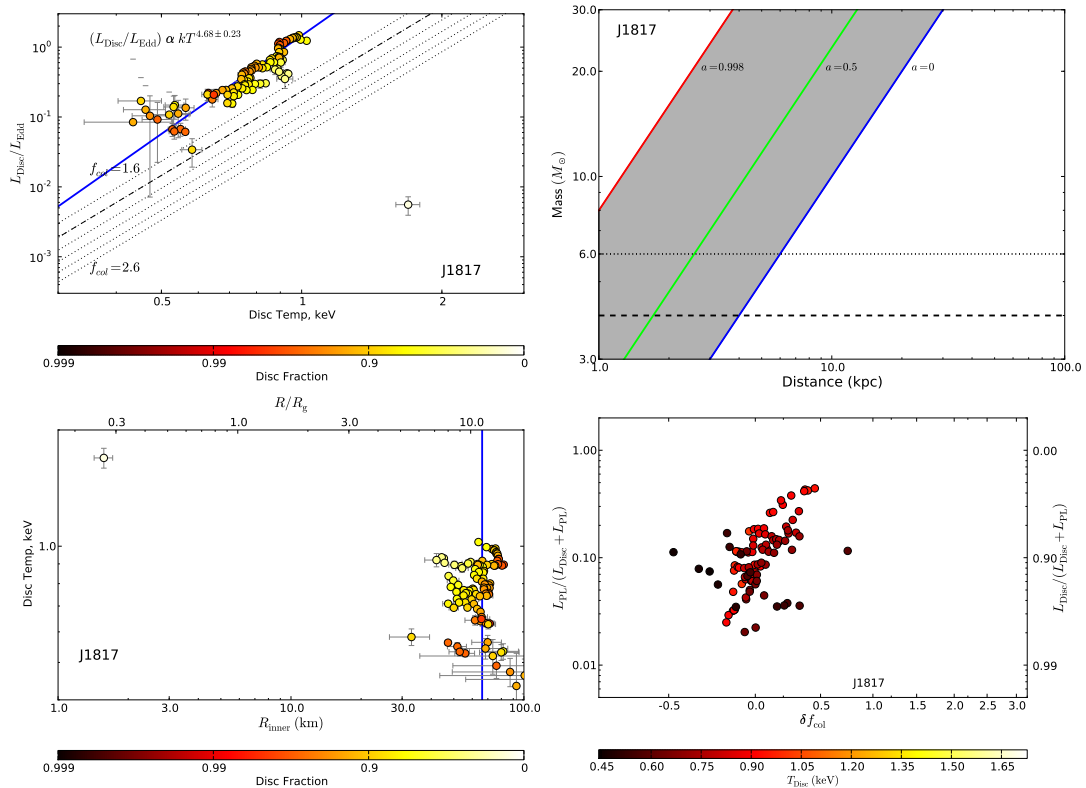


Figure A.1. (cont) XTE J1817-330

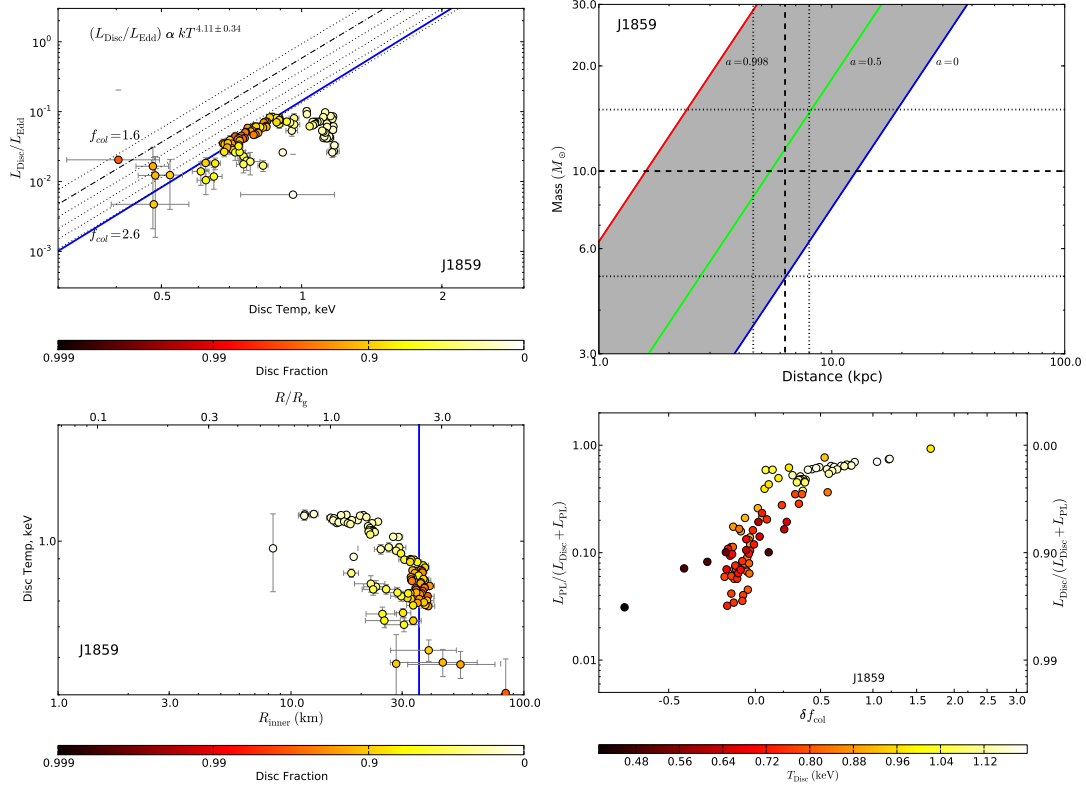


Figure A.1. (cont) XTE J1859+226

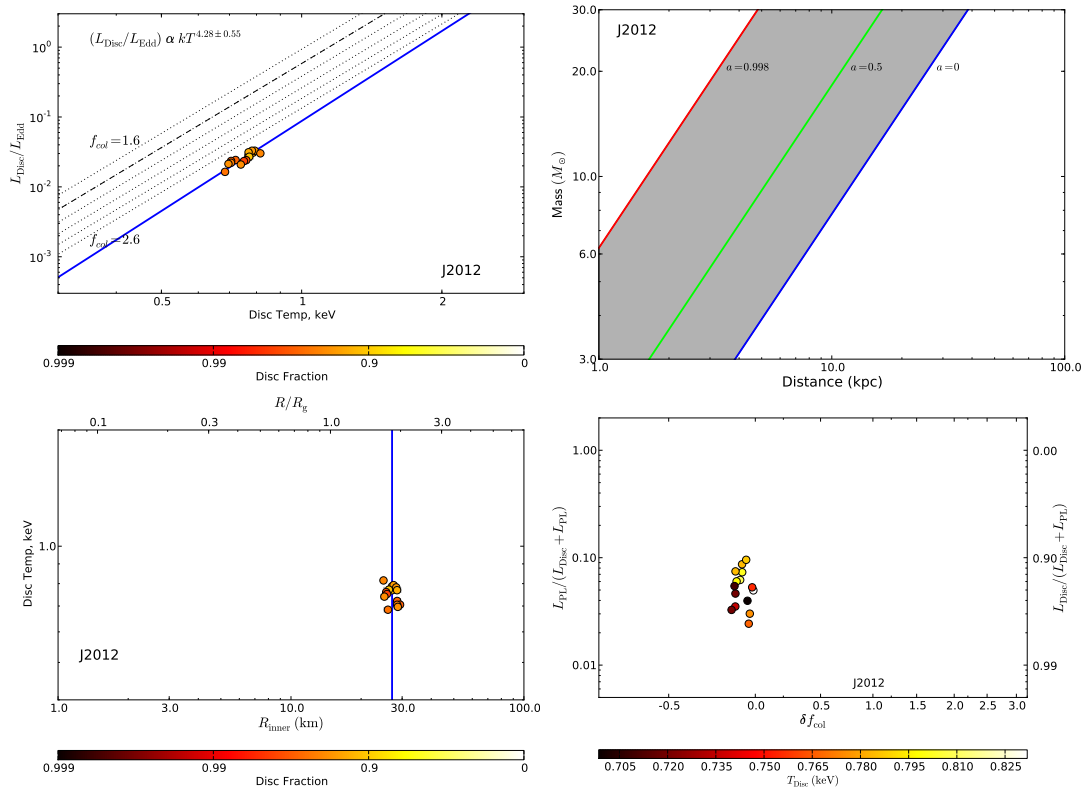


Figure A.1. (cont) XTE J2012+381

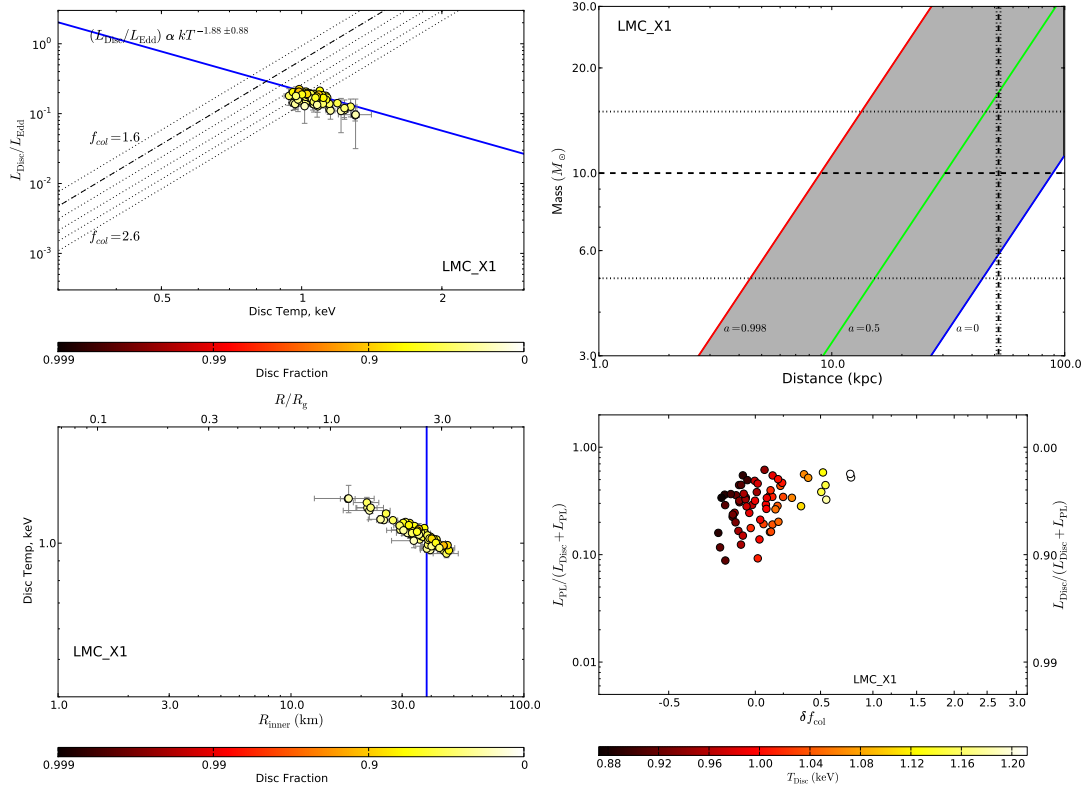


Figure A.1. (cont) LMC X-1

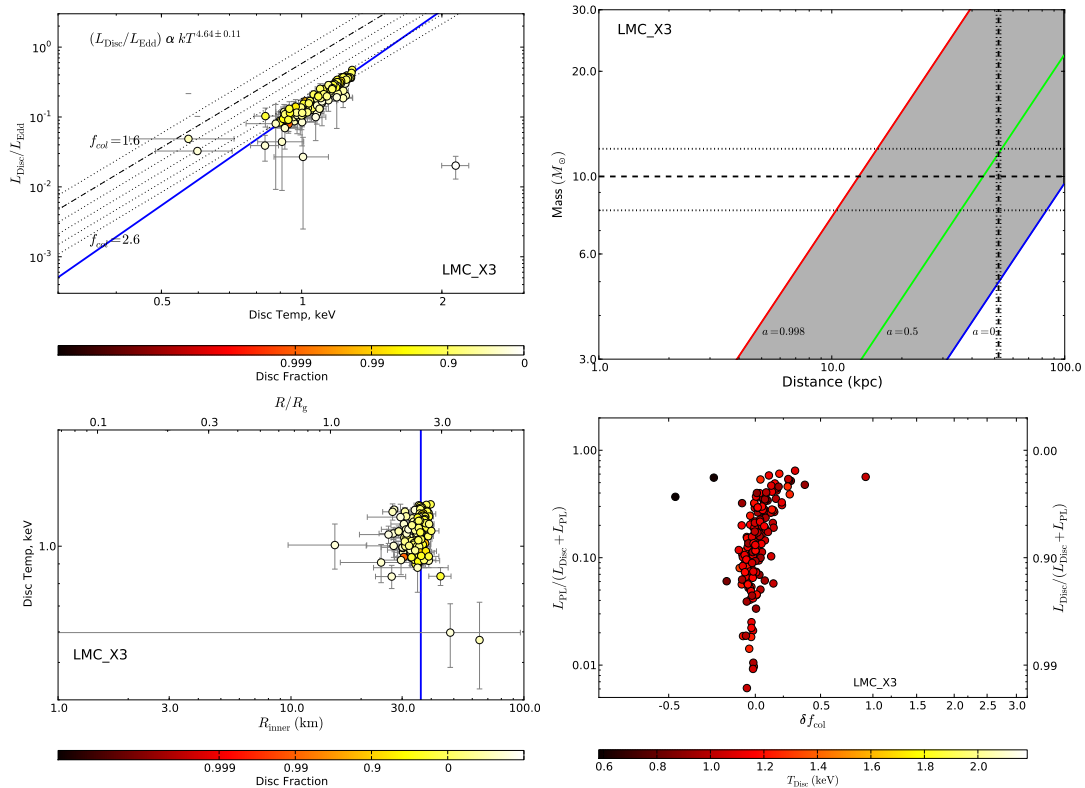


Figure A.1. (cont) LMC X-3

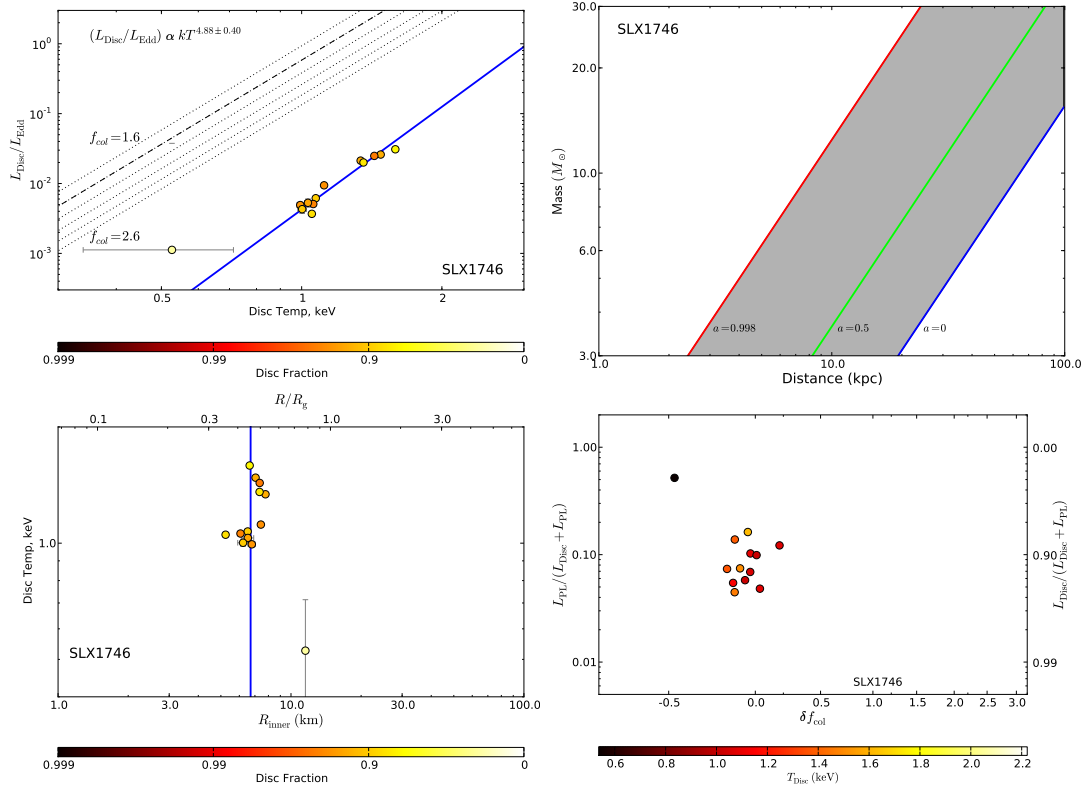


Figure A.1. (cont) SLX 1746-331

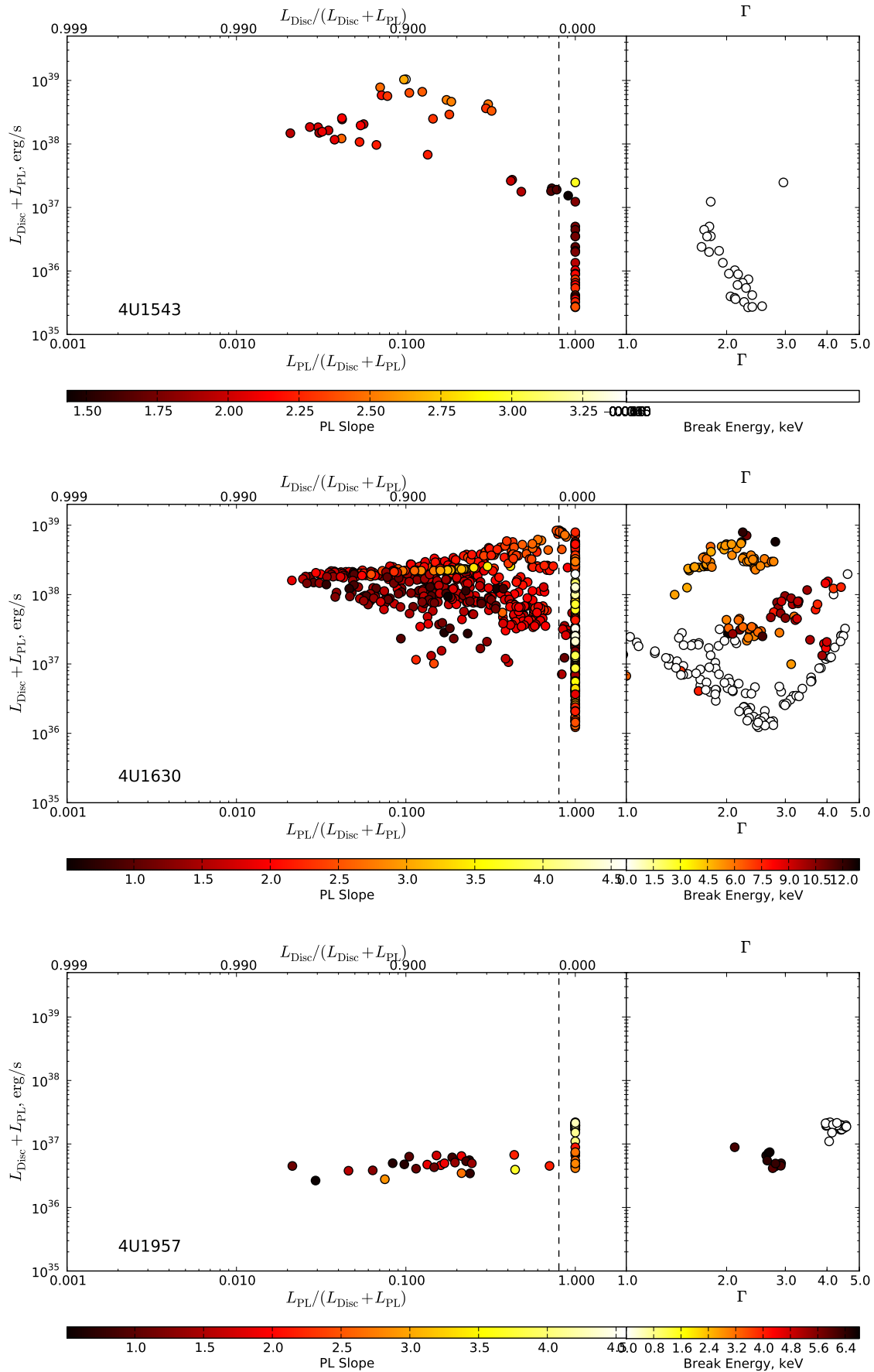


Figure A.2. The DFLDs with the colour scale showing the powerlaw slope. Also shown in the side panel is the powerlaw slope (below the break where appropriate) for the observations with a disc fraction < 0.2, along with the break energy for the broken powerlaw (where it occurs). TOP: 4U 1543-47, MIDDLE: 4U 1630-47, BOTTOM: 4U 1957+115.

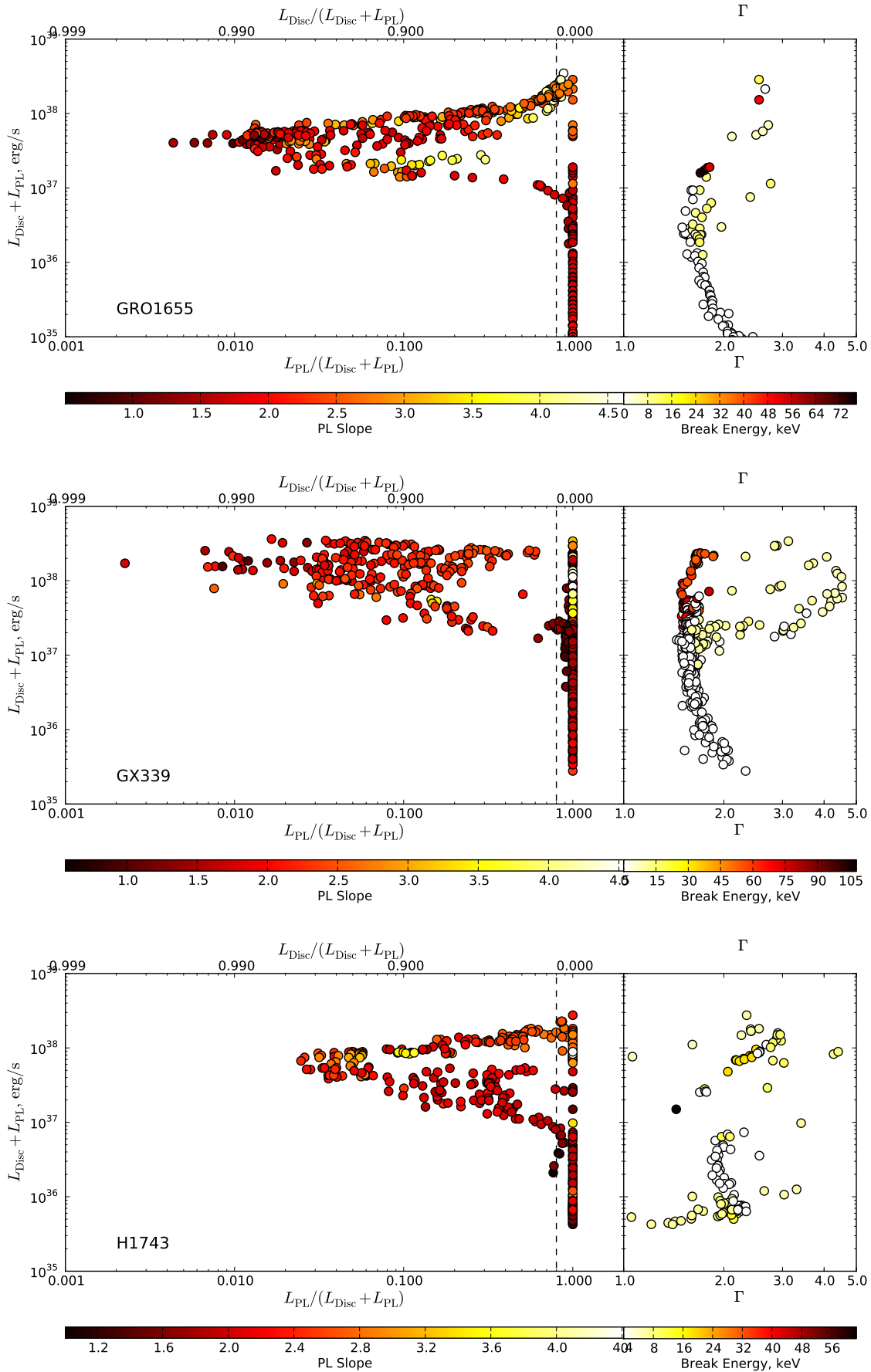
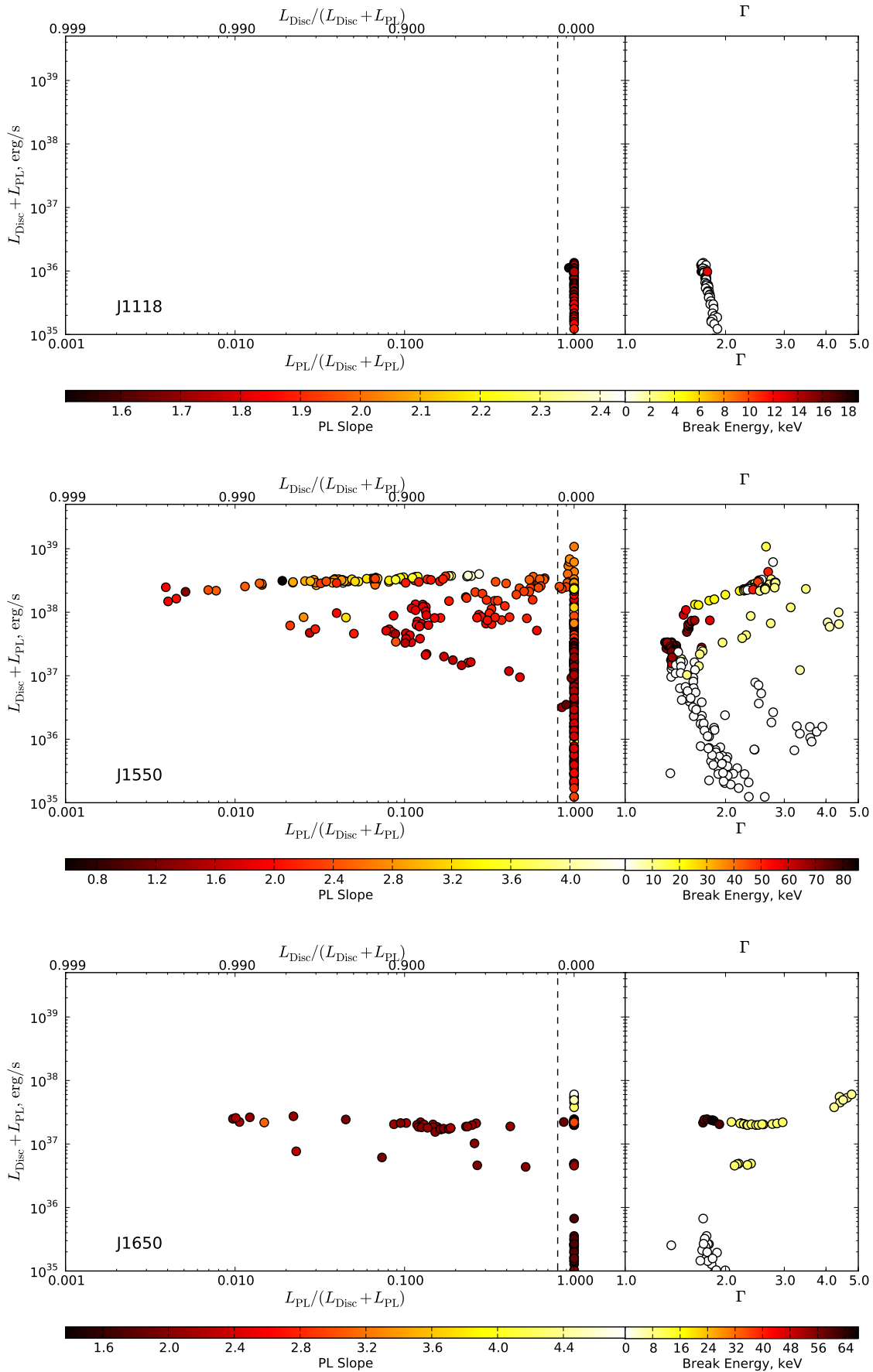


Figure A.2. (cont) TOP: GRO J1655-40, MIDDLE: GX 339-4, BOTTOM: H 1743-322. © 0000 RAS, MNRAS 000, 000-000



© 0000 RAS, MNRAS 000, 000–000 **Figure A.2.** (cont) TOP: XTE J1118+480, MIDDLE: XTE J1550-564, BOTTOM: XTE J1650-500.

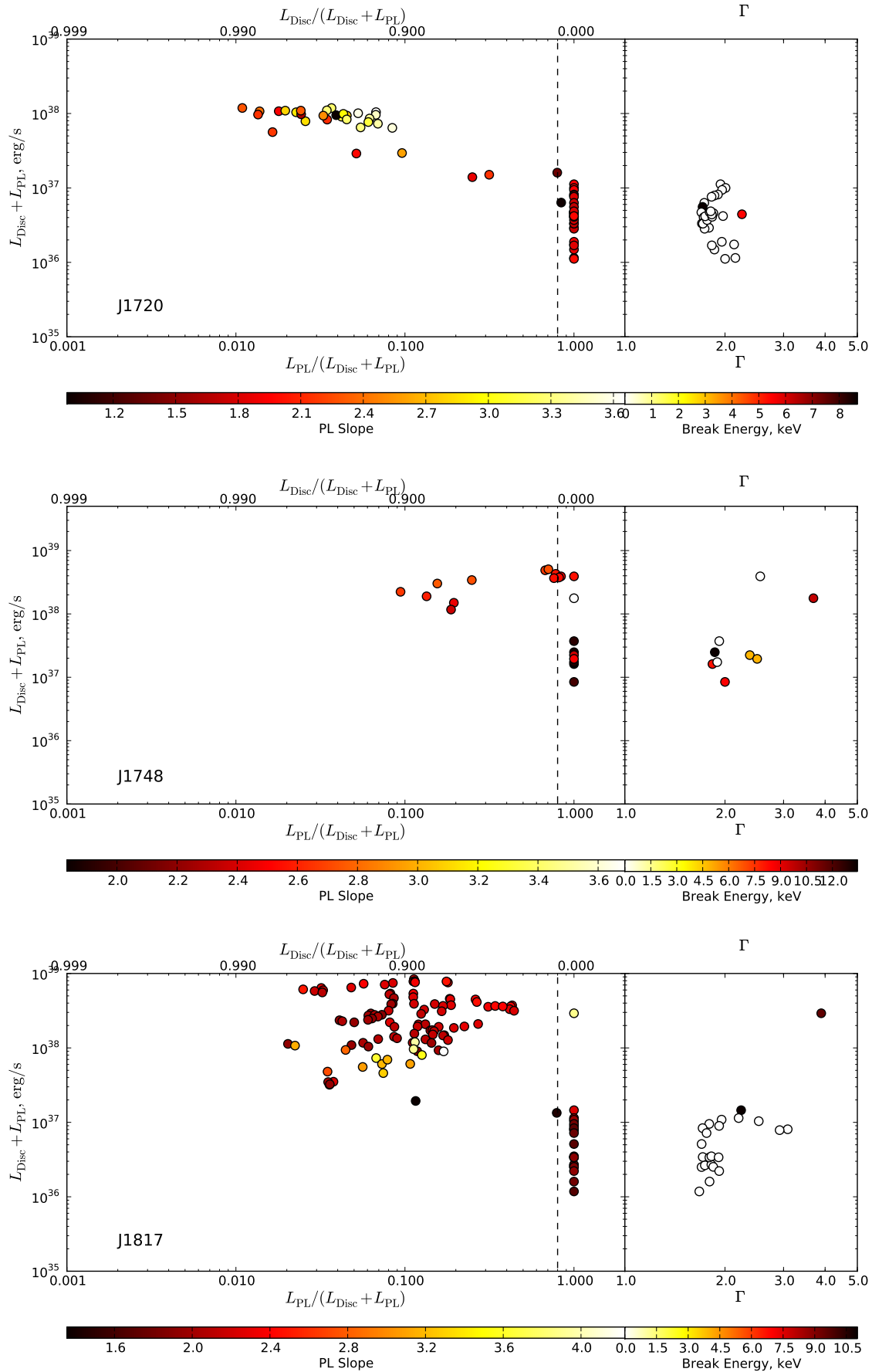


Figure A.2. (cont) TOP: XTE J1720-318, MIDDLE: XTE J1748-288, BOTTOM: XTE J1817-330
 © 0000 RAS, MNRAS 000, 000-000

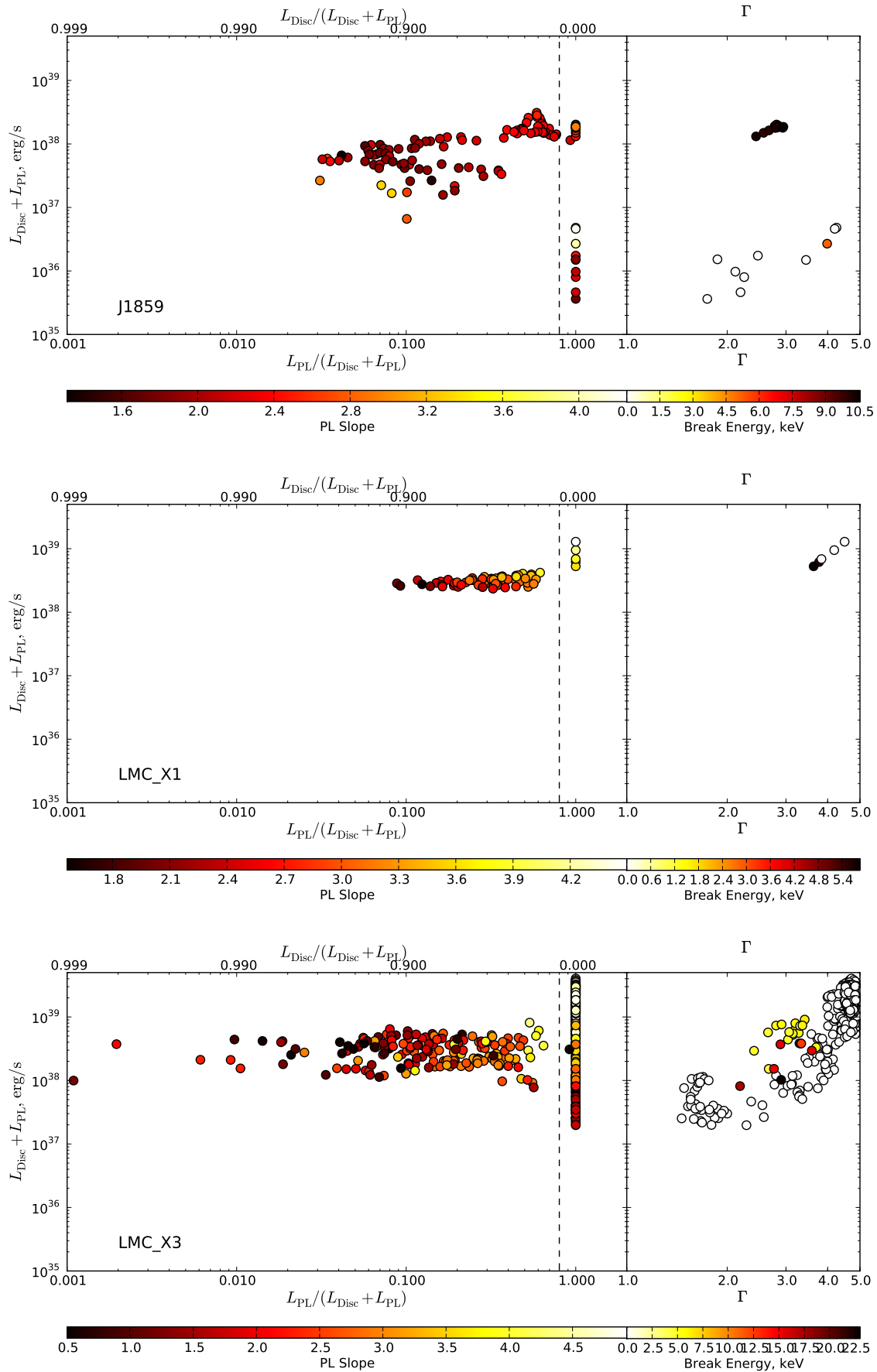


Figure A.2. (cont) TOP: XTE J1859+226, MIDDLE: LMC X-1, BOTTOM: LMC X-3.

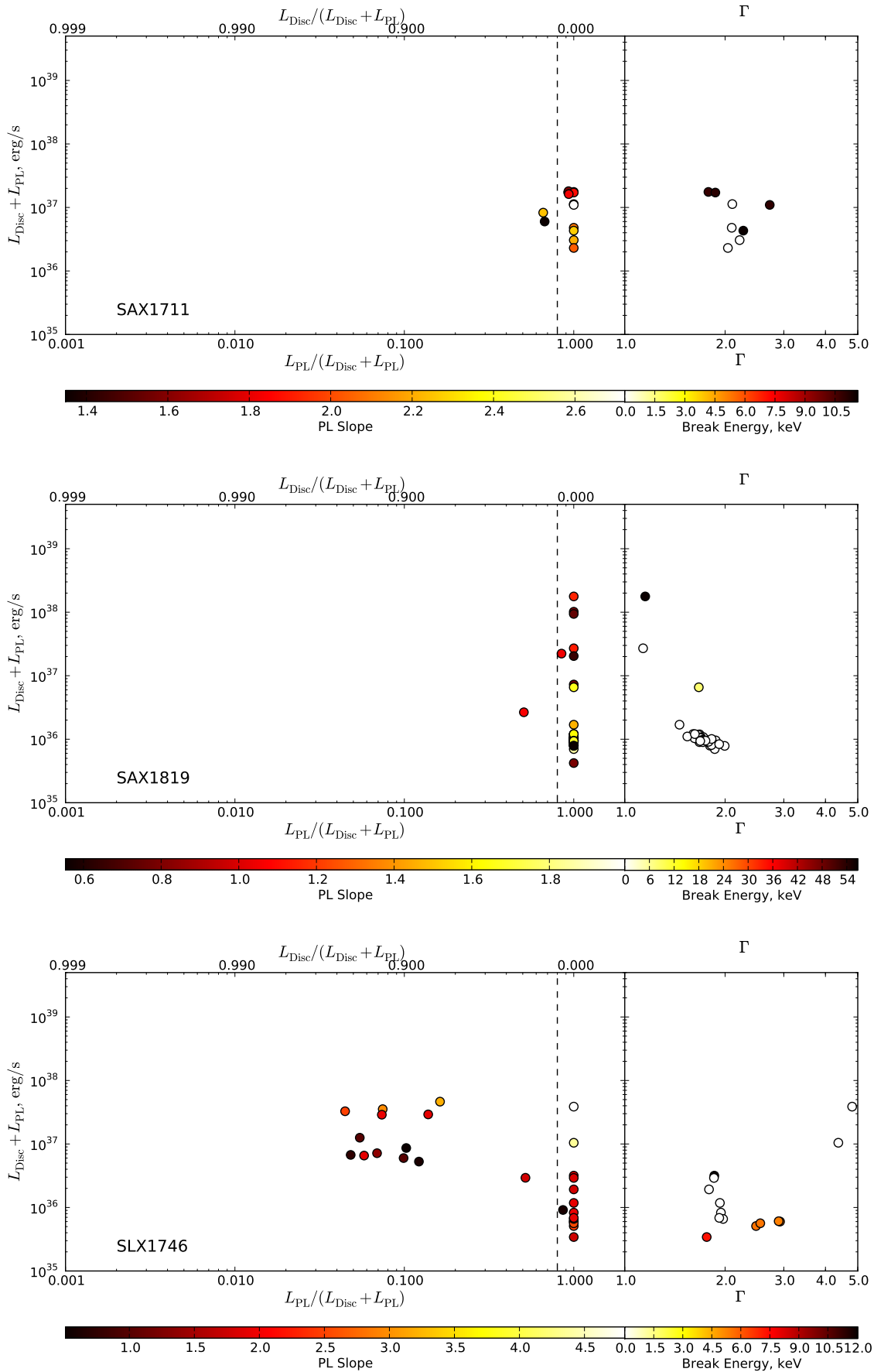


Figure A.2. (cont) TOP: SAX 1711.6-3808, MIDDLE: SAX 1918.3-2525, BOTTOM: SLX 1746-331
 © 0000 RAS, MNRAS 000, 000-000

